Journal Pre-proofs

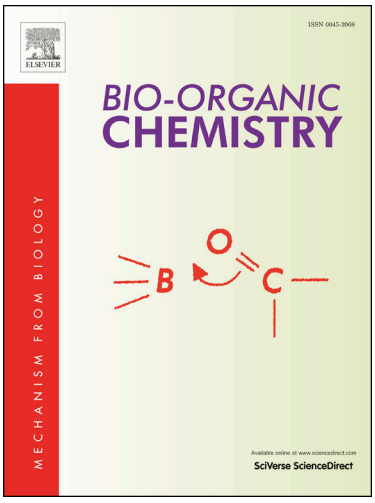

Molecular Mechanism of Action of New 1,4-Naphthoquinones tethered to 1,2,3-1*H*-Triazoles with Cytotoxic and Selective Effect Against Oral Squamous Cell Carcinoma

Ingrid Cavalcanti Chipoline, Anna Carolina Carvalho da Fonseca, Gabriella Ribeiro Machado da Costa, Michele Pereira de Souza, Vitor Won-Held Rabelo, Lucas N. de Queiroz, Theo Luiz Ferraz de Souza, Elan Cardozo Paes de Almeida, Paula Alvarez Abreu, Bruno Pontes, Vitor Francisco Ferreira, Fernando de Carvalho da Silva, Bruno K. Robbs

PII: S0045-2068(20)31281-5
DOI: https://doi.org/10.1016/j.bioorg.2020.103984
Reference: YBIOO 103984

To appear in: *Bioorganic Chemistry*

Received Date: 5 March 2020
Revised Date: 27 April 2020
Accepted Date: 29 May 2020

Please cite this article as: I. Cavalcanti Chipoline, A. Carolina Carvalho da Fonseca, G. Ribeiro Machado da Costa, M. Pereira de Souza, V. Won-Held Rabelo, L.N. de Queiroz, T. Luiz Ferraz de Souza, E. Cardozo Paes de Almeida, P. Alvarez Abreu, B. Pontes, V. Francisco Ferreira, F. de Carvalho da Silva, B.K. Robbs, Molecular Mechanism of Action of New 1,4-Naphthoquinones tethered to 1,2,3-1*H*-Triazoles with Cytotoxic and Selective Effect Against Oral Squamous Cell Carcinoma, *Bioorganic Chemistry* (2020), doi: https://doi.org/10.1016/j.bioorg.2020.103984

Molecular Mechanism of Action of New 1,4-Naphthoquinones tethered to 1,2,3-1*H*-Triazoles with Cytotoxic and Selective Effect Against Oral Squamous Cell Carcinoma

Ingrid Cavalcanti Chipoline,[a,‡] Anna Carolina Carvalho da Fonseca,[b,‡] Gabriella Ribeiro Machado da Costa,[c] Michele Pereira de Souza,[d] Vitor Won-Held Rabelo,[e] Lucas N. de Queiroz,[d] Theo Luiz Ferraz de Souza,[f] Elan Cardozo Paes de Almeida,[c] Paula Alvarez Abreu,[e] Bruno Pontes,[g] Vitor Francisco Ferreira,[h] Fernando de Carvalho da Silva,[a,*] Bruno K. Robbs[b,**]

[a] Universidade Federal Fluminense, Departamento de Química Orgânica, Instituto de Química, Campus do Valonguinho, CEP 24020-150, Niterói-RJ, Brasil.
[b] Universidade Federal Fluminense, Programa de Pós-graduação em Odontologia, Instituto de Saúde de Nova Friburgo, CEP 28625-650, Nova Friburgo-RJ, Brasil.
[c] Universidade Federal Fluminense, Campus Universitário de Nova Friburgo, Departamento de Ciência Básica, CEP 28625-650, Nova Friburgo-RJ, Brasil.
[d] Universidade Federal Fluminense, Programa de Pós-Graduação em Ciências Aplicadas a Produtos para Saúde, Faculdade de Farmácia, Niterói-RJ, Brasil.
[e] Universidade Federal do Rio de Janeiro, Instituto de Biodiversidade e Sustentabilidade, Campus Macaé, CEP 27965-045, Macaé-RJ, Brasil.
[f] Universidade Federal do Rio de Janeiro, Faculdade de Farmácia, CEP 21941-902, Rio de Janeiro-RJ, Brasil.
[g] Universidade Federal do Rio de Janeiro, Instituto de Ciências Biomédicas, CEP 21941-902, Rio de Janeiro-RJ, Brasil.
[h] Universidade Federal Fluminense, Faculdade de Farmácia, Departamento de Tecnologia Farmacêutica, CEP 24241-000, Niterói-RJ, Brasil.

‡ Authors contributed equally

Corresponding authors:

Chemistry: **Fernando de Carvalho da Silva**, Universidade Federal Fluminense, Departamento de Química Orgânica, Instituto de Química, Campus do Valonguinho, CEP 24020-150, Niterói-RJ, Brasil; E-mail: fcsilva@id.uff.br

Biological Assays: **Bruno K. Robbs**, Universidade Federal Fluminense, Programa de Pós-graduação em Odontologia, Instituto de Saúde de Nova Friburgo, CEP 28625-650, Nova Friburgo-RJ, Brasil. E-mail: brunokr@id.uff.br

Abstract

The oral squamous cell carcinoma (OSCC) stands out as a public health problem due to its high incidence and low survival rate, despite advances in diagnosis and treatment. Moreover, the most commonly chemotherapeutic agents for OSCC, such as carboplatin and cisplatin, generate important side effects, evidencing the urgency in developing new drugs. Naphthoquinones are an important class of natural products or synthetic compounds with cytotoxic effect demonstrated on different cancer types. In the present study, thirty-five 1,4-naphthoquinones tethered to 1,2,3-1*H*-triazoles were synthesized and the antitumor activity and molecular mechanisms were evaluated in several assays including *in vitro* and *in vivo* models of OSCC and normal oral human cells. Compounds **16a**, **16b** and **16g** were able to induce cytotoxicity in three different tumor cell lines of human OSCC (SCC4, SCC9 and SCC25) and were more toxic and selective to tumor cells (Selective Index, SI > 2) than classical and chemically similar controls (Carboplatin and Lapachol). Compound **16g** showed the higher SI value. Besides, compounds **16a**, **16b** and **16g** significantly reduced colony formation of SCC9 cells in the tested concentrations. Hemolytic assay using compounds **16a**, **16b** and **16g** at high concentrations showed no compound exhibited hemolysis higher than 5%, similar to controls. *In vivo* acute toxicity study showed that **16g** was the only one, among the three compounds, with no apparent limiting toxic effects on mice in the tested concentrations. Thus, the investigation of cell death mechanisms was conducted with this compound. **16g** does not trigger ROS production nor binds to DNA. On the other hand, compound **16g** induced microtubule disorganization, and molecular modeling studies suggests a potential mechanism of action related to inhibition of topoisomerases and/or hPKM2 activities. Cell morphology, pyknotic nuclei presence, cleaved caspase-3 staining and viability assays using caspase-3 inhibitors demonstrate compound **16g** induced cell death through apoptosis. Among the 35 synthesized triazole naphthoquinones, compound **16g** was the most effective compound against OSCC cells, presenting high cytotoxicity (~ 35 μM), selectivity (SI ~ 6) and low acute toxicity on animals, and therefore might be considered for future cancer therapy.

Keywords: Lapachol; lawsone; CuAAC; multicomponent reactions; OSCC; hemolysis.

1. Introduction

Oral squamous cell carcinoma (OSCC) is the eighth most common cancer in men [1] with 345,864 new cases and 177,384 deaths occurring only in 2018 worldwide [2]. The disease is more common in males above 60 years and the overall 5-year survival rate of OSCC is approximately 60 %, varying between 80 % for stage I cancers and 40 % for stage IV cancers [1]. OSCC accounts for more than 90 % of all oral cancers and is characterized by invasive growth, being frequently associated with regional metastases at diagnosis [3]. The main causative factors of the disease are alcohol, tobacco products and human papillomavirus (HPV) infection [4].

The treatment of OSCC can be performed through chemotherapy, radiotherapy and surgery. Platinum compounds such as carboplatin and cisplatin are the most commonly used in chemotherapy in conjunction with other antineoplastic agents. Side effects include renal failure, gastrointestinal problems, neurotoxicity and acquired resistance, thus justifying the search for new substances with antineoplastic effects that overcome the side effects and the high costs of the current treatments [5, 6].

Naphthoquinones are substances derived from quinones that are present in fungi and algae plants [7]. In addition, naphthoquinones have been shown to be useful in the development of health products, presenting antimalarial [8], antiparasitic [9, 10], bactericidal [11] and antifungal [12] actions. The relevance of these substances in the production of compounds with antineoplastic activity is due to their ability to produce a partial redox cycle generating reactive oxygen species (ROS) in the tumor cell, causing an oxidative stress and consequently the cell death. In addition, when interacting with the enzyme topoisomerase, naphthoquinones inhibit their activity in processes such as DNA replication, repair and transcription [13]. In the present study, thirty five compounds of 1,4-naphthoquinones tethered to 1,2,3-1*H*-triazoles were synthesized and antitumor activity and molecular mechanisms evaluated in a series of assays including *in vitro* and *in vivo* models of OSCC and normal oral human cells.

2. Experimental Section

2.1. Chemistry

The reagents were purchased from Sigma-Aldrich Brazil and were used without further purification. Column chromatography was performed with silica gel 60 (Merck 70-230 mesh). Analytical thin layer chromatography was performed with silica gel plates (Merck, TLC silica gel 60 F_{254}), and the plates were visualized using UV light. The indicated yields refer to homogeneous materials purified by chromatography and confirmed by spectroscopic techniques. Melting points were obtained on a Thermo scientific 9100 apparatus and were uncorrected. Infrared spectra were collected using KBr pellets on a Perkin-Elmer model 1420 FT-IR spectrophotometer, and the spectra were calibrated relative to the 1601.8 cm^{-1} absorbance of polystyrene. ^{1}H and ^{13}C NMR were recorded at room temperature using a Varian VXR Unity 300 or 500 MHz, in the DMSO-d_6. Chemical shifts (δ) are given in ppm and coupling constants (*J*) in Hertz. The chemical shift data were reported in units of δ (ppm) downfield from solvent, and the solvent was used as an internal standard; coupling constants (*J*) are reported in hertz and refer to apparent peak multiplicities. High-resolution mass spectra (HRMS) were recorded on a MICROMASS Q-TOF mass spectrometer (Waters).

The protocols of *C*-alkylation for preparing the quinones **2-5** [14-18], the *O*-alkylation to obtain **6-8** [19, 20] and the all arylazides [21, 22] respective physical and spectroscopic data were previously reported in literature.

*2.1.1. General procedure for the preparation of **9** e **10***

A 100 mL round-bottom flask containing a solution of **4** or **5** (4.38 mmols), K_2CO_3 (5.3 mmols) in 50 mL of acetone was stirred for 15 minutes, then 10 eq of propargyl bromide was added and reflux lasting for 12 h. After, the solvent was evaporated under reduced pressure, the residue was solubilized in ethyl acetate and washed with water (3 x 50 mL), the organic phase was dried with anhydrous sodium sulfate and the solvent was evaporated under reduced pressure. The product was purified by column chromatography containing silicagel using gradient hexane:ethyl acetate as eluent.

(E)-2-(3-methylbut-1-en-1-yl)-3-(prop-2-yn-1-yloxy)naphthalene-1,4-dione (**9**). Yellow solid, 75 % yield, m.p. 100-101 ºC. IR (KBr, cm^{-1}) ν: 2360, 2960, 2871, 2124, 1711, 1661, 1620, 1592,

1330, 1291, 1267, 1251, 1190, 1157, 1043, 974, 934, 715, 665. ^{1}H NMR (DMSO-d_6, 300.00 MHz) δ ppm: 8.00-7.96 (2H, m), 7.85-7.82 (2H, m), 7.08 (1H, dd, *J* 7.1 and 16.2 Hz), 6.51 (1H, dd, *J* 1.4 and 16.2 Hz), 5.11 (2H, d, *J* 2.4 Hz), 3.60 (1H, td, *J* 2.4 Hz), 2.56-2.44 (1H, m), 1.08 (6H, d, *J* 6.7 Hz) ppm. HR-ESIMS [M+Na] *m/z* calcd. for $C_{18}H_{16}NaO_3$: 303.0992. Found: 303.0986 m/z. Δ = 2 ppm.

2-allyl-3-(prop-2-yn-1-yloxy)naphthalene-1,4-dione (**10**). Yellow solid, 60 % yield, m.p. 110-111 ºC. IR (KBr, cm^{-1}) ν: 3270, 2122, 1668, 1652, 1611, 1590, 1331, 1295, 1262, 1226, 1184, 1155, 1042, 1028, 995, 960, 968, 918, 908, 894, 721, 663, 648, 607. ^{1}H NMR (DMSO-d_6, 300.00 MHz) δ ppm: 8.02-7.98 (2H, m), 7.86-7.83 (2H, m), 5.86 (1H, dddd; *J* 6.3, 10.0 and 16.4 Hz), 5.15-5.14 (3H, m); 5.02 (1H, dd, *J* 1.5 and 10.0 Hz), 3.59 (1H, t, *J* 2.3 Hz), 3.30 (2H, dt, *J* 1.5 and 6.3 Hz). HR-ESIMS [M+Na] *m/z* calcd. for $C_{16}H_{12}NaO_3$: 275.0679. Found: 275.0670 m/z. Δ = 3.3 ppm.

*2.1.2. General procedure for the preparation of **13-17***

In a 100 mL round-bottom flask containing a solution of arylazide **12a-g** (0.5 mmol), 1,4-naphthoquinone **6-10** (0.8 mmol), 16 mL of distilled water, 8 mL of CH_2Cl_2 and 8 mL of *t*-BuOH were added $CuSO_4.5H_20$ (1.1 mmol), sodium ascorbate (0.18 mmol) and acetic acid (1.7 μmol). After 10 hours, the product was extracted from aqueous phase with dichloromethane(2 x 20 mL), the organic phase was dried with anhydrous sodium sulfate and the solvent evaporated under reduced pressure. The product was purified by column chromatography containing silicagel using gradient hexane:ethyl acetate as eluent.

2-((1-(4-chlorophenyl)-1H-1,2,3-triazol-4-yl)methoxy)naphthalene-1,4-dione (**13a**). Yellow solid, 30 % yield, m.p. 232-234 °C. IR (KBr, cm^{-1}) ν: 3142, 3108, 3063, 1678, 1651, 1597, 1578, 1240, 1201, 1173, 1162, 1090, 1038, 1023, 1009, 989, 866, 832, 779, 716, 704, 553, 527. ^{1}H NMR (DMSO-d_6, 500.00 MHz) δ ppm: 8.96 (1H, s), 8.02-7.98 (2H, m), 7.95 (2H, d, *J* 8.9 Hz), 7.88-7.80 (2H, m), 7.66 (2H, d, *J* 8.9 Hz), 6.64 (1H, s), 5.37 (2H, s). ^{13}C NMR (DMSO-d_6, 125.0 MHz APT) δ ppm: 189.6, 184.6, 164.1, 147.4, 140.6, 139.6, 138.8, 138.5, 136.8, 136.1, 135.0. HR-ESIMS [M+Na] *m/z* calcd. for $C_{19}H_{12}ClN_3O_3Na$: 388.0459. Found: 388.0457. Δ = 0.5 ppm.

2-((1-(2,5-dichlorophenyl)-1H-1,2,3-triazol-4-yl)methoxy)naphthalene-1,4-dione (**13b**). Yellow solid, 75 % yield, m.p. 200-201 °C. IR (KBr, cm^{-1}) ν: 3077, 3057, 1684, 1655, 1614, 1591, 1578, 1489, 1455, 1359, 1334, 1308, 1259, 1250, 1212, 1122, 1097, 1039, 1019, 999, 873, 828, 817, 807, 720. ^{1}H NMR (DMSO-d_6, 500.00 MHz) δ ppm: 8.76 (1H, s,), 8.03-7.99 (2H, m), 7.92 (1H, d, *J* 2,0 Hz), 7.88-7.83 (2H, m), 7.80 (1H, d, *J* 8.7 Hz), 7.72 (1H, dd, *J* 2.0 and 8.7 Hz), 6.66 (1H, s), 5.39 (2H, s). ^{13}C NMR (DMSO-d_6, 125.0 MHz APT) δ ppm: 184.8, 179.8, 159.4, 141.7, 135.8, 134.9, 134.0, 133.0, 132.3, 132.0, 132.0, 131.4, 128.6, 128.0, 127.9, 126.5, 128.99, 111.7, 62.6. HR-ESIMS [M+Na] *m/z* calcd. for $C_{19}H_{11}Cl_2N_3O_3Na$: 422.0075.; Found: 422.0064. Δ = 2.1 ppm.

2-((1-(2-chlorophenyl)-1H-1,2,3-triazol-4-yl)methoxy)naphthalene-1,4-dione (**13c**). Yellow solid, 70 % yield, m.p. 162-163 ºC. IR (KBr, cm^{-1}) ν: 3162, 1679, 1652, 1605, 1594, 1578, 1491, 1457, 1348, 1332, 1303, 1266, 1242, 1205, 1037, 1012, 865, 787, 763, 726. ^{1}H NMR (DMSO-d_6, 500.00 MHz) δ ppm: 8.71 (1H, s), 8.00-7.99 (3H, m), 7.80 (1H, d, *J* 2.0 Hz), 7.70-7.68 (2H, m), 7.60 (1H, d, *J* 8.7 Hz), 7.52 (1H, dd, *J* 2.5 and 8.5 Hz), 6.65 (1H, s), 5.38 (2H, s). ^{13}C NMR (DMSO-d_6, 125.0 MHz APT) δ ppm: 184.1, 179.1, 158.7, 140.8, 134.1, 133.3, 131.4, 131.2, 130.6, 130.3, 128.3, 128.1, 128.1, 127.1, 125.8, 125.3, 110.9, 62.0. HR-ESIMS [M+Na] *m/z* calcd. for $C_{19}H_{12}ClN_3O_3Na$: 388.0459. Found: 388.0453. Δ = 1.5 ppm.

2-((1-(3,4-dichlorophenil)-1H-1,2,3-triazol-4-il)metoxy)naphthaleno-1,4-dione (**13d**). Yellow solid, 83 % yield, m.p. 156-157 °C. IR (KBr, cm^{-1}) ν: 1678, 1648, 1608, 1487, 1331, 1308, 1246, 1206, 1138, 1086, 1039, 1000, 880, 818, 778, 720. ^{1}H NMR (DMSO-d_6, 500.00 MHz) δ ppm: 9.04 (1H, s), 8.25 (1H, d; *J* 2.5 Hz), 8.03-7.99 (2H, m), 7.96 (1H, dd, *J* 2.5 and 8.7 Hz), 7.87-7.81 (3H, m), 6.64 (1H, s), 5.38 (2H, s). ^{13}C NMR (DMSO-d_6, 125.0 MHz APT) δ ppm: 184.0, 179.1, 158.5, 142.1, 135.7, 134.1, 133.3, 132.1, 131.4, 131.3, 131.0, 130.6, 125.7, 125.2, 123.5, 121.8, 120.1, 110.8, 61.9. HR-ESIMS [M+Na] *m/z* calcd. for $C_{19}H_{11}Cl_2N_3O_3Na$: 422.0075. Found: 422.0051. Δ = 5.7 ppm.

2-((1-phenil-1H-1,2,3-triazol-4-yl)metoxy)naphthaleno-1,4-dione (**13e**). Yellow Solid, 82 % yield, m.p. 176-178 °C. IR (KBr, cm^{-1}) ν: 3135, 1660, 1644, 1608, 1504, 1332, 1307, 1269, 1232,

1191, 1039, 1009, 866, 843, 783, 758, 723, 687. ^{1}H NMR (DMSO-d_6, 500.00 MHz) δ ppm: 8.94 (1H, s), 8.03-7.99 (2H, m), 7.91 (2H, dd, *J* 1.1 and 8.6 Hz), 7.88-7.81 (2H, m), 7.86 (1H, td, *J* 1.5 and 7.4 Hz), 7.82 (1H, td, *J* 1.5 and 7.4 Hz), 7.63-7.60 (2H, m), 7.53-7.54 (1H, m), 6.65 (1H, s), 5.38 (2H, s). ^{13}C NMR (DMSO-d_6, 125.0 MHz APT) δ ppm: 184.1, 179.1, 158.6, 141.8, 136.2, 134.1, 133.2, 131.3, 130.6, 129.5, 128.5, 125.7, 125.2, 123.3, 120.1, 110.8, 62.0, 54.4. HR-ESIMS [M+Na] *m/z* calcd. for $C_{19}H_{13}N_3O_3Na$: 354.0855. Found: 354.0836. Δ = 5.4 ppm.

2-((1-(3,5-dichlorophenyl)-1H-1,2,3-triazol-4-yl)methoxy)naphthalene-1,4-dione (**13f**). Yellow solid, 92 % yield, m.p. 215-216 °C. IR (KBr, cm^{-1}) ν: 3157, 3079, 1681, 1652, 1591, 1481, 1450, 1336, 1307, 1247, 1202, 1156, 1038, 1012, 884, 852, 831, 804, 783. ^{1}H NMR (DMSO-d_6, 500.00 MHz) δ ppm: 9.07 (1H, s), 8.06 (2H, d, *J* 1.7 Hz), 8.03-7.98 (2H, m), 7.88-7.81 (2H, m), 7.73 (1H, s), 6.62 (1H, s), 5.38 (2H, s). ^{13}C NMR (DMSO-d_6, 125.0 MHz APT) δ ppm: 184.0, 179.0, 158.5, 142.1, 137.8, 134.9, 134.1, 133.2, 131.3, 130.6, 127.9, 125.7, 125.2, 123.6, 118.8, 110.9, 61.9. HR-ESIMS [M+Na] *m/z* calcd. for $C_{19}H_{11}Cl_2N_3O_3Na$: 422.0075. Found: 422.051. Δ = 5.7 ppm.

2-((1-(3-chlorophenyl)-1H-1,2,3-triazol-4-yl)methoxy)naphthalene-1,4-dione (**13g**). Yellow solid, 77 % yield, m.p. 202-203 °C. IR (KBr, cm^{-1}) ν: 3154, 1660, 1656, 1607, 1090, 1331, 1308, 1266, 1238, 1200, 1037, 1011, 866, 784, 723, 683. ^{1}H NMR (DMSO-d_6, 500.00 MHz) δ ppm: 9.02 (1H, s), 8.04-7.99 (3H, m), 7.93-7.91 (1H, m), 7.88-7.81 (2H, m), 7.64 (1H, t, *J* 8.1 Hz), 7.58-7.56 (1H, m), 6.64 (1H, s), 5.38 (2H, s). ^{13}C NMR (DMSO-d_6, 125.0 MHz APT) δ ppm: 184.1, 179.1, 158.6, 141.9, 137.3, 134.1, 134.0, 133.3, 131.3, 131.2, 130.6, 128.4, 125.8, 123.5, 120.0, 118.7, 110.9 62.0. HR-ESIMS [M+Na] *m/z* calcd. for $C_{19}H_{12}ClN_3O_3Na$: 388.0459. Found: 388.0442. Δ = 4.4 ppm.

2-((1-(4-chlorophenyl)-1H-1,2,3-triazol-4-yl)methoxy)-3-(2-metilprop-1-en-1-yl)naphthalene-1,4-dione (**14a**). Orange solid, 63 % yield, m.p. 109-110 °C. IR (KBr, cm^{-1}) ν: 3089, 2963, 2916, 1651, 1594, 1501, 1445, 1376, 1330, 1293, 1260, 1192, 1144, 1094, 1043, 976, 831, 800, 726. ^{1}H NMR (DMSO-d_6, 500.00 MHz) δ ppm: 8.86 (1H, s), 8.04-7.96 (2H, m), 7.93 (2H, d, *J* 8.7 Hz), 7.85-7.83 (2H, m), 7.66 (2H, d, *J* 8.7 Hz), 5.81 (1H, s), 5.43 (2H, s), 1.83 (3H, s), 1.49 (3H, s). ^{13}C NMR (DMSO-d_6, 125.0 MHz APT) δ ppm: 185.0, 181.4, 155.6, 144.4, 142.5, 135.8, 134.6, 134.2,

133.5, 132.1, 131.7, 131.5, 130.3, 126.3, 126.3, 123.4, 122.2, 115.2, 65.4, 26.5, 21.7. HR-ESIMS [M+Na] *m/z* calcd. for $C_{23}H_{18}ClN_3O_3Na$: 442.0934. Found: 442.0923. Δ = 2.5 ppm.

2-((1-(2,5-dichlorophenyl)-1H-1,2,3-triazol-4-yl)methoxy)-3-(2-metilprop-1-en-1-yl)naphthalene-1,4-dione (**14b**). Orange solid, 34 % yield, m.p. 110-111 °C. IR (KBr, cm^{-1}) ν: 3149, 2924, 1653, 1595, 1437, 1453, 1385, 1297, 1261, 1226, 1184, 1096, 1039, 1021, 959, 923, 885, 846, 821, 791, 718, 673. ^{1}H NMR (DMSO-d_6, 500.00 MHz) δ ppm: 8.61 (1H, s), 8.03-8.02 (1H, m), 7.98-7.96 (1H, m), 7.85-7.83 (3H, m), 7.79 (1H, d, = 8.7 Hz), 7.72 (1H, dd, *J* 2.5 and 8.7 Hz), 5.82 (1H, m), 5.47 (2H, s), 1.86 (3H, d, *J* 1.0 Hz), 1.54 (3H, d, *J* 1.0 Hz). ^{13}C NMR (DMSO-d_6, 125.0 MHz APT) δ ppm: 184.3, 180.9, 154.8, 142.7, 133.9, 133.5, 132.3, 131.7, 131.4, 131.3, 131.1, 131.0, 127.8, 127.3, 126.6, 125.6, 114.6, 89.3, 64.6, 25.8, 21.1. HR-ESIMS [M+Na] *m/z* calcd. for $C_{23}H_{17}Cl_2N_3O_3Na$·: 476.0539. Found: 476.0560. Δ = 4.4 ppm.

2-((1-(2-chlorophenyl)-1H-1,2,3-triazol-4-yl)methoxy)-3-(2-metylprop-1-en-1-yl)naphthalene-1,4-dione (**14c**). Orange solid, 54 % yield, m. p. 110-111 °C. IR (KBr, cm^{-1}) ν: 2906, 1666, 1592, 1566, 1498, 1486, 1332, 1303, 1267, 1206, 1073, 1037, 1009, 964, 931, 890, 805, 748, 718, 661. ^{1}H NMR (DMSO-d_6, 500.00 MHz) δ ppm: 8.57 (1H, s), 8.04-7.96 (2H, m), 7.85-7.83 (2H, m), 7.75 (1H, d, *J* 7.8 Hz), 7.66-7.57 (3H, m), 5.81 (1H, s), 5.47 (2H, s), 1.86 (3H, s), 1.53 (3H, s). ^{13}C NMR (DMSO-d_6, 125.0 MHz APT) δ ppm: 184.9, 181.5, 155.5, 143.3, 142.4, 134.9, 134.5, 134.1, 132.2, 132.0, 131.8, 131.7, 131.0, 129.0, 128.9, 128.8, 128.6, 127.1, 126.3, 115.2, 65.4, 26.4, 21.7. HR-ESIMS [M+Na] *m/z* calcd. for $C_{23}H_{18}ClN_3O_3Na$: 442.0929. Found: 442.0928. Δ = 0.2 ppm.

2-((1-(3,4-dichlorophenyl)-1H-1,2,3-triazol-4-yl)methoxy)-3-(2-metylprop-1-en-1-yl)naphthalene-1,4-dione (**14d**). Orange solid, 88 % yield, m.p. 136-137 °C. IR (KBr, cm^{-1}) ν: 3099, 2992, 1665, 1594, 1488, 1438, 1379, 1327, 1293, 1261, 1193, 1133, 1040, 1002, 968, 879, 811, 768, 720, 677, 650. ^{1}H NMR (DMSO-d_6, 500.00 MHz) δ ppm: 8.23 (1H, s), 8.22 (1H, d, *J* 2.3 Hz), 8.03-7.93 (3H, m), 7.86-7.83 (3H, m), 5.83 (1H, s), 5.43 (2H, s), 1.85 (3H, s), 1.51 (3H, s). ^{13}C NMR (DMSO-d_6, 125.0 MHz APT) δ ppm: 184.4, 181.0, 155.1, 144.1, 142.0, 136.1, 134.0, 133.6, 132.4, 131.8, 131.7, 131.3, 131.2, 125.8, 125.8, 121.9, 120.2, 114.7, 64.9, 25.9, 21.2. HR-ESIMS [M+Na] *m/z* calcd. for $C_{23}H_{17}Cl_2N_3O_3Na$: 476.0539. Found: 476.0534. Δ = 1.0 ppm.

2-(2-methylprop-1-en-1-yl)-3-((1-phenyl-1H-1,2,3-triazol-4-yl)methoxy)naphthalene-1,4-dione (**14e**). Orange solid, 60 % yield, m.p. 100-101 °C. IR (KBr, cm^{-1}) ν: 3092, 2911, 1667, 1651, 1593, 1572, 1503, 1453, 1323, 1304, 1267, 1229, 1214, 1193, 1076, 1043, 1022, 961, 927, 848, 757, 726, 713, 698, 669, 646. ^{1}H NMR (DMSO-d_6, 500.00 MHz) δ ppm: 8.83 (1H, s), 8.05-7.94 (2H, m), 7.90-7.91 (4H, m), 7.63-7.56 (2H, m), 7.51-7.48 (1H, m), 5.81 (1H, m), 5.43 (2H, s), 1.83 (3H, d, *J* 2.2 Hz), 1.49 (3H, d, *J* 1.7 hz). ^{13}C NMR (DMSO-d_6, 125.0 MHz APT) δ ppm: 184.2, 180.7, 154.9, 143.6, 141.6, 136.3, 133.8, 133.4, 131.4, 131.0, 129.5, 125.5, 125.5, 122.4, 119.9, 114.4, 95.0, 65.2, 64.8, 25.6, 20.9. HR-ESIMS [M+Na] *m/z* calcd. for $C_{23}H_{19}N_3O_3Na$: 408.1319. Found: 408.1305. Δ = 3.4 ppm.

2-((1-(3,5-dichlorophenyl)-1H-1,2,3-triazol-4-yl)methoxy)-3-(2-metylprop-1-en-1-yl)naphthalene-1,4-dione (**14f**). Orange solid, 70 % yield, m.p. 115-116 °C. IR (KBr, cm^{-1}) ν: 3086, 2969, 2930, 1670, 1646, 1595, 1574, 1480, 1440, 1329, 1305, 1259, 1189, 1047, 985, 848, 805, 728, 719, 668. ^{1}H NMR (DMSO-d_6, 500.00 MHz) δ ppm: 8.99 (1H, s), 8.05-8.02 (3H, m), 7.98-7.96 (1H, m), 7.85-7.83 (2H, m), 7.74-7.73 (1H, m), 5.82 (1H, s), 5.43 (2H, s), 1.84 (3H, d, *J* 1.0 Hz), 1.51 (3H, s). ^{13}C NMR (DMSO-d_6, 125.0 MHz APT) δ ppm: 184.1, 180.7, 154.7, 143.8, 141.7, 137.9, 135.0, 133.8, 133.3, 131.4, 131.0, 130.9, 127.8, 125.5, 125.5, 122.9, 118.5, 188.3, 114.4, 64.6, 25.6, 20.9. HR-ESIMS [M+Na] *m/z* calcd. for $C_{23}H_{17}Cl_2N_3O_3Na$: 476.0539. Found: 476.0520. Δ = 4.0 ppm.

2-((1-(3-chlorophenyl)-1H-1,2,3-triazol-4-yl)methoxy)-3-(2-metylprop-1-en-1-yl)naphthalene-1,4-dione (**14g**). Orange solid, 60 % yield, m.p. 101-102 °C. IR (KBr, cm^{-1}) ν: 3124, 3098, 2912, 1687, 1652, 1595, 1675, 1430, 1341, 1327, 1310, 1294, 1259, 1193, 1097, 1043, 1024, 969, 914, 787, 727, 677. ^{1}H NMR (DMSO-d_6, 500.00 MHz) δ ppm: 8.93 (1H, s), 8.04-8.01 (2H, m), 7.98-7.96 (1H, m), 7.91-7.89 (1H, m), 7.85-7.83 (2H, m), 7.62 (1H, *t*, *J* 8.1 Hz), 7.57-7.55 (1H, m), 5.82-5.81 (1H, m), 5.43 (2H, s), 1.84 (3H, d, *J* 1.2 Hz), 1.50 (3H, d, *J* 0.8 Hz). ^{13}C NMR (DMSO-d_6, 125.0 MHz APT) δ ppm: 184.9, 181.5, 155.6, 144.5, 142.4, 138.1, 134.7, 134.5, 134.1, 132.2, 132.0, 131.8, 131.7, 139.0, 126.3, 126.2, 123.4, 120.4, 119.2, 115.2, 65.5, 26.4, 21.7. HR-ESIMS [M+Na] *m/z* calcd. for $C_{23}H_{18}ClN_3O_3Na$: 442.0929. Found: 442.0922. Δ = 1.6 ppm.

2-((1-(4-chlorophenyl)-1H-1,2,3-triazol-4-yl)methoxy)-3-(3-metylbut-2-en-1-yl)naphthalene-1,4-dione (**15a**). Orange solid, 40 % yield, m.p. 150-151 °C. IR (KBr, cm^{-1}) ν: 3087, 2987, 2909, 1656, 1609, 1593, 1579, 1501, 1459, 1331, 1306, 1259, 1239, 1211, 1190, 1092, 1048, 949, 932, 827, 790, 722, 641. ^{1}H NMR (DMSO-d_6, 500.00 MHz) δ ppm: 8.88 (1H, s), 8.04-8.02 (1H, m), 7.98-7.96 (1H, m), 7.90 (2H, d, *J* 8.8 Hz), 7.84-7.82 (2H, m), 7.64 (2H, d, *J* 8.8 Hz), 5.56 (2H, s), 4.89-4.86 (1H, m), 3.11 (2H, d, *J* 7.2 Hz), 1.58 (3H, s), 1.50 (3H, s). ^{13}C NMR (DMSO-d_6, 125.0 MHz APT) δ ppm: 185.0, 181.6, 156.5, 144.4, 135.8, 135.1, 134.6, 134.1, 133.6, 132.8, 132.0, 131.7, 130.3, 126.4, 126.2, 123.4, 122.3, 120.5, 65.8, 25.7, 23.2, 18.0. HR-ESIMS [M+Na] *m/z* calcd. for $C_{24}H_{20}ClN_3O_3Na$: 456.1031. Found: 456.1064. Δ = 7.2 ppm.

2-((1-(2,5-dichlorophenyl)-1H-1,2,3-triazol-4-yl)methoxy)-3-(3-metylbut-2-en-1-yl)naphthalene-1,4-dione (**15b**). Orange solid, 33 % yield, m.p. 102-104 °C. IR (KBr, cm^{-1}) ν: 3142, 3100, 3074, 2970, 2924, 1674, 1644, 1601, 1575, 1485, 1457, 1378, 1329, 1302, 1263, 1237, 1204, 1195, 1095, 1060, 1044, 1010, 995, 948, 937, 870, 826, 819, 807, 720, 591, 576, 529. ^{1}H NMR (DMSO-d_6, 500.00 MHz) δ ppm: 8.64 (1H, s), 8.03-8.01 (1H, m), 7.98-7.96 (1H, m), 7.83-7.92 (2H, m), 7.80 (1H, d, *J* 2.5 Hz), 7.76 (1H, d, *J* 8.7 Hz), 7.69 (1H, dd, *J* 2.5 and 8.7 Hz), 5.58 (2H, s), 4.98 (1H, ddd, *J* 1.0, 4.2 and 7.1 Hz), 3.11 (2H, d, *J* 7.1 Hz), 1.62 (2H, s), 1.57 (3H, d, *J* 1.0 Hz). ^{13}C NMR (DMSO-d_6, 125.0 MHz APT) δ ppm: 185.0, 181.6, 156.4, 143.4, 135.2, 134.6, 134.2, 133.0, 133.0, 132.4, 131.9, 131.7, 128.4, 127.9, 127.3, 126.4, 126.2, 120.5, 65.7, 25.7, 23.2, 18.1. HR-ESIMS [M+Na] *m/z* calcd. for $C_{24}H_{19}Cl_2N_3O_3Na$: 490.0701. Found: 490.0676. Δ = 1.0 ppm.

2-((1-(2-chlorophenyl)-1H-1,2,3-triazol-4-yl)methoxy)-3-(3-metilbut-2-en-1-yl)naphthalene-1,4-dione (**15c**). Orange solid, 73 % yield, m.p. 80-82 °C. IR (KBr, cm^{-1}) ν: 3125, 3084, 2952, 2927, 1656, 1593, 1578, 1493, 1458, 1375, 1332, 1261, 1238, 1191, 1048, 949, 934, 847, 789, 755, 720, 703. ^{1}H NMR (DMSO-d_6, 500.00 MHz) δ ppm: 8.61 (1H, s), 8.05-8.03 (1H, m), 8.00-7.98 (1H, m), 7.85-7.83 (2H, m), 7.74 (1H, dd, *J* 1.5 and 8.1 Hz), 7.66-7.58 (3H, m), 5.61 (2H, s), 5.01-4.98 (1H, m), 3.12 (2H, d, *J* 7.2 Hz), 1.64 (3H, s), 1.58 (3H, d, *J* 1.0 Hz). ^{13}C NMR (DMSO-d_6, 125.0 MHz APT) δ ppm: 185.0, 181.6, 156.5, 143.2, 135.2, 134.9, 134.6, 134.2, 132.9, 132.1, 132.0,

131.7, 131.0, 128.9, 128.9, 128.6, 127.3, 126.4, 126.2, 120.5, 65.8, 25.7, 23.2, 18.1. HR-ESIMS [M+H] *m/z* calcd. for $C_{24}H_{21}ClN_3O_3$: 434.1266. Found: 434.1249. Δ = 3.9 ppm.

2-((1-(3,4-dichlorophenyl)-1H-1,2,3-triazol-4-yl)methoxy)-3-(3-metylbut-2-en-1-yl)naphthalene-1,4-dione (**15d**). Orande solid, 71 % yield, m.p. 124-126 °C. IR (KBr, cm^{-1}) ν: 3133, 2905, 1666, 1651, 1594, 1577, 1485, 1438, 1335, 1235, 1211, 1193, 1129, 1057, 1041, 1023, 953, 876, 824, 721, 679, 584. ^{1}H NMR (DMSO-d_6, 500.00 MHz) δ ppm: 8.99 (1H, s), 8.23 (1H, d, *J* 2.5 Hz), 8.05-8.04 (1H, m), 8.00-7.98 (1H, m), 7.94 (1H, dd, *J* 2.5 and 8.7 Hz), 7.86-7.84 (3H, m), 5.57 (2H, s), 4.92-4.89 (1H, m), 3.13 (2H, d, *J* 7.2 Hz), 1.61 (3H, s), 1.53 (3H, s). ^{13}C NMR (DMSO-d_6, 125.0 MHz APT) δ ppm: 185.0, 181.6, 156.5, 143.2, 135.2, 134.9, 134.6, 134.2, 132.9, 132.0, 132.0, 131.7, 131.0, 128.9, 128.6, 127.3, 126.4, 126.2, 120.5, 65.8, 25.7, 23.2, 18.1. HR-ESIMS [M+Na] *m/z* calcd. for $C_{24}H_{19}Cl_2N_3O_3Na$: 490.0696. Found: 490.0702. Δ = 1.2 ppm.

2-(3-metylbut-2-en-1-yl)-3-((1-phenyl-1H-1,2,3-triazol-4-yl)methoxy)naphthalene-1,4-dione (**15e**). Orange solid, 77 % yield, m.p. 139-140 °C. IR (KBr, cm^{-1}) ν: 3073, 2910, 1664, 1663, 1610, 1593, 1500, 1334, 1263, 1240, 1108, 1061, 956, 952, 761, 722, 689. ^{1}H NMR (DMSO-d_6, 500.00 MHz) δ ppm: 8.87 (1H, s), 8.06-8.04 (1H, m), 8.00-7.98 (1H, m), 7.89-7.87 (2H, m), 7.86-7.84 (2H, m), 7.61-7.58 (2H, m), 7.51-7.48 (1H, m), 5.58 (2H, s), 4.91-4.88 (1H, m), 3.13 (2H, d, *J* 7.2 Hz), 1.60 (3H, s), 1.52 (3H, s). ^{13}C NMR (DMSO-d_6, 125.0 MHz APT) δ ppm: 185.0, 181.6, 156.4, 136.5, 135.1, 134.6, 134.1, 132.9, 132.9, 132.2, 132.0, 131.7, 131.7, 126.4, 126.2, 123.6, 122.3, 120.6, 120.5, 65.7, 25.7, 23.2, 18.0. HR-ESIMS [M+Na] *m/z* calcd. for $C_{24}H_{21}N_3O_3Na$: 422.1475. Found: 422.1466. Δ = 1.2 ppm.

2-((1-(3,5-diclorofenil)-1H-1,2,3-triazol-4-il)metoxi)-3-(3-metilbut-2-en-1-il)naftaleno-1,4-diona (**15f**). Orange solid, 78 % yield, m.p. 103-104 °C. IR (KBr, cm^{-1}) ν: 3081, 2961, 2919, 1659, 1651, 1591, 1479, 1439, 1332, 1259, 1239, 1190, 1048, 1010, 949, 930, 849, 800, 719, 666. ^{1}H NMR (DMSO-d_6, 500.00 MHz) δ ppm: 9.03 (1H, s), 8.06-8.03 (3H, m), 8.00-7.98 (1H, m), 7.86-7.84 (2H, m), 7.72 (1H, t, *J* 1.7 Hz), 5.57 (2H, s), 4.93-4.90 (1H, m), 3.13 (2H, d, *J* 7.8 Hz), 1.61 (3H, s), 1.53 (3H, d, *J* 1.0 Hz). ^{13}C NMR (DMSO-d_6, 125.0 MHz APT) δ ppm: 185.1, 181.6, 156.6, 144.3, 137.1, 135.1, 134.6, 134.2, 132.9, 132.0, 131.8, 130.3, 129.2, 126.4, 126.2, 132.4, 121.3,

120.6, 120.5, 65.9, 25.7, 23.2, 18.0. HR-ESIMS [M+Na] *m/z* calcd. for $C_{24}H_{19}Cl_2N_3O_3Na$: 490.0696. Found: 490.0646. Δ = 10.2 ppm.

2-((1-(3-chlorophenyl)-1H-1,2,3-triazol-4-yl)methoxy)-3-(3-metylbut-2-en-1-yl)naphthalene-1,4-dione (**15g**). Orange solid, 73 % yield, m.p. 142-143 °C. IR (KBr, cm^{-1}) ν: 3135, 3100, 2958, 2912, 1689, 1654, 1608, 1596, 1490, 1333, 1260, 1240, 1193, 1058, 1049, 953, 784, 720, 677. ^{1}H NMR (DMSO-d_6, 500.00 MHz) δ ppm: 8.96 (1H, s), 8.06-8.04 (1H, m), 8.01-7.97 (2H, m), 7.90 (1H, ddd, *J* 1.0, 2.0 and 8.1 Hz), 7.86-7.83 (2H, m), 7.64-7.61(1H, m), 7.56 (1H, ddd, *J* 1.0, 2.0 and 8.1 Hz), 5.58 (2H, s), 4.91-4.89 (1H, m), 3.13 (2H, d, *J* 7.2 Hz), 1.60 (3H, s), 1.52 (3H, d, *J* 0.8 Hz). ^{13}C NMR (DMSO-d_6, 125.0 MHz APT) δ ppm: 185.0, 181.6, 156.4, 144.6, 138.7, 135.8, 135.2, 134.6, 134.2, 132.9, 132.0, 131.7, 128.6, 126.4, 126.2, 123.8, 120.5, 119.3, 65.7, 25.7, 23.2, 18.0. HR-ESIMS [M+Na] *m/z* calcd. for $C_{24}H_{20}ClN_3O_3Na$: 456.1031. Found: 456.1064. Δ = 7.2 ppm.

2-((1-(4-chlorophenyl)-1H-1,2,3-triazol-4-yl)methoxy)-3-(3-metylbut-1-en-1-yl)naphthalene-1,4-dione (**16a**). Red solid, 81 % yield, m.p. 144-145 °C. IR (KBr, cm^{-1}) ν: 3099, 2906, 2867, 1659, 1624, 1545, 1501, 1332, 1304, 1292, 1252, 1197, 1094, 1047, 963, 933, 830, 790, 714. ^{1}H NMR (DMSO-d_6, 500.00 MHz) δ ppm: 8.93 (1H, s), 8.05-7.98 (2H, m), 7.91 (2H, d, *J* 8.9 Hz), 7.86-7.83 (2H, m), 7.66 (2H, d, *J* 8.9 Hz). 6.90 (1H, dd, *J* 7.0 and 16.3 Hz), 6.33 (1H, dd, *J* 1.1 and 16.3 Hz), 5.56 (2H, s), 2.35 (1H, ddq, *J* 1.1, 6.7 and 7.0 Hz), 0.92 (6H, d, *J* 6.7 Hz). ^{13}C NMR (DMSO-d_6, 125.0 MHz APT) δ ppm: 185.0, 181.6, 156.5, 144.4, 138.1, 135.1, 134.7, 134.6, 134.2, 132.8, 132.0, 132.0, 131.7, 129.0, 126.4, 126.2, 123.5, 120.5, 120.4, 119.2, 65.8, 25.7, 23.2, 18.0. HR-ESIMS [M+H] *m/z* calcd. for $C_{24}H_{21}ClN_3O_3$: 434.1266. Found: 434.1243. Δ = 5.3 ppm.

2-((1-(2,5-dichloropheniyl)-1H-1,2,3-triazol-4-yl)methoxy)-3-(3-metylbut-1-en-1-yl)naphthalene-1,4-dione (**16b**). Red solid, 33 % yield, m.p. 102-104 °C. IR (KBr, cm^{-1}) ν: 2954, 2923, 2867, 1666, 1591, 1551, 1488, 1336, 1292 1184, 1101, 1022, 962, 930, 878, 822, 723, 591. ^{1}H NMR (DMSO-d_6, 500.00 MHz) δ ppm: 8.69 (1H, s), 8.02-8.01 (1H, m), 7.98-7.97 (1H, m), 7.84-7.83 (2H, m); 7.81-7.78 (2H, m), 7.71 (1H, dd, *J* 2.5 and 8.7 Hz), 6.95 (1H, dd, *J* 7.1 and 16.3 Hz), 6.35 (1H, dd, *J* 1.1 and 16.3 Hz), 5.60 (2H, s), 2.37 (1H, ddq, *J* 1.1, 6.7 and 7.1Hz), 0.97 (6H, d, *J* 6.7 Hz). ^{13}C NMR (DMSO-d_6, 125.0 MHz APT) δ ppm: 185.2, 181.4, 155.1, 150.5,

144.3, 135.8, 134.5, 134.2, 133.6, 132.2, 131.7, 130.3, 129.5, 126.4, 126.1, 123.5, 122.2, 116.6, 66.1, 32.9, 22.1, 22.1. HR-ESIMS [M+Na] *m/z* calcd. for $C_{24}H_{19}Cl_2N_3O_3Na$: 490.07016. Found: 490.0683. Δ = 5.3 ppm.

2-((1-(2-chlorophenyl)-1H-1,2,3-triazol-4-yl)methoxy)-3-(3-metylbut-1-en-1-yl)naphthalenr-1,4-dione (**16c**). Red solid, 30 % yield, m.p. 69-71 °C. IR (KBr, cm^{-1}) ν: 3133, 2905, 1666, 1651, 1577, 1485, 1438, 1335, 1235, 1193, 1129, 1057, 1041, 1023, 953, 934, 876, 824, 795, 721, 679. ^{1}H NMR (DMSO-d_6, 500.00 MHz) δ ppm: 8.61 (1H, s), 8.04-8.02 (1H, m), 8.00-7.98 (1H, m), 7.86-7.83 (2H, m), 7.75-7.73 (1H, m), 7.64-7.57 (3H, m), 6.95 (1H, dd, *J* 7.0 and 16.3 Hz), 6.38 (1H, dd, *J* 1.4 and 16.3 Hz), 5.62 (1H, s), 2.40 (1H, ddq, *J* 1.4, 6.8 and 7.0 Hz), 0.99 (6H, d, *J* 6.8 Hz). ^{13}C NMR (DMSO-d_6, 125.0 MHz APT) δ ppm: 184.4, 180.6, 154.3, 149.8, 142.4, 133.8, 133.4, 133.2, 132.2, 131.6, 131.5, 131.1, 130.9, 128.9, 127.6, 127.1, 126.6, 125.6, 125.3, 65.1, 32.2, 21.4. HR-ESIMS [M+Na] *m/z* calcd. for $C_{24}H_{21}ClN_3O_3$: 456.1091. Found: 456.1073. Δ = 3.9 ppm.

2-((1-(3,4-dichlorophenyl)-1H-1,2,3-triazol-4-yl)methoxy)-3-(3-metylbut-1-en-1-yl)naphthalene-1,4-dione (**16d**). Red solid, 34 % yield, m.p. 102-103 °C. IR (KBr, cm^{-1}) ν: 3144, 2969, 1662, 1620, 1591, 1489, 1348, 1293, 1260, 1191, 1138, 1043, 1000, 964, 923, 651, 809, 719, 676. ^{1}H NMR (DMSO-d_6, 500.00 MHz) δ ppm: 8.99 (1H, s), 8.20 (1H, d, *J* 2.5 Hz), 8.04-8.01 (1H, m), 8.01-7.99 (1H, m), 7.93 (1H, dd, *J* 2.5 and 8.8 Hz), 7.87-7.84 (3H, m), 6.92 (1H, dd, *J* 1.4 and 16.3 Hz), 6.36 (1H, dd, *J* 1.4 and 16.3 Hz), 5.56 (2H, s), 2.37 (1H, ddq, *J* 1.4, 6.8 and 7.0 Hz), 0.95 (6H, d, *J* 6.8 Hz). ^{13}C NMR (DMSO-d_6, 125.0 MHz APT) δ ppm: 185.1, 181.4, 181.4, 155.1, 150.5, 143.1, 134.5, 134.2, 132.2, 132.0, 131.7, 131.0, 129.6, 128.9, 128.9, 128.8, 128.7, 128.6, 126.3, 124.4, 124.1, 65.9, 55.4, 32.9, 22.6, 22.2. HR-ESIMS [M+Na] *m/z* calcd. for $C_{24}H_{19}Cl_2N_3O_3Na$: 490.0716. Found: 490.0684. Δ = 6.5 ppm.

2-(3-metylbut-1-en-1-yl)-3-((1-phenyl-1H-1,2,3-triazol-4-yl)methoxy)naphthalene-1,4-dione (**16e**) . Red solid, 73 % yield, m.p. 100-101 °C. IR (KBr, cm^{-1}) ν: 3146, 2957, 2869, 1661, 1648, 1622, 1593, 1503, 1354, 1332, 1302, 1268, 1252, 1198, 1047, 962, 759, 721, 689. ^{1}H NMR (DMSO-d_6, 500.00 MHz) δ ppm: 8.87 (1H, s), 8.05-8.03 (1H, m), 8.01-7.99 (1H, m), 7.87-7.84 (4H, m), 7.61-7.58 (2H, m), 7.51-7.48 (1H, m), 6.91 (1H, dd, *J* 7.0 and 16.3 Hz), 6.35 (1H, dd, *J*

1.4 and 16.3 Hz), 5.57 (2H, s), 2.36 (1H, ddq, *J* 1.4, 6.8 and 7.0 Hz), 0.94 (6H, d, *J* 6.8 Hz). ^{13}C NMR (DMSO-d_6, 125.0 MHz APT) δ ppm: 185.1, 181.4, 155.1, 150.6, 144.5, 136.5, 134.6, 134.2, 132.9, 132.3, 132.3, 132.2, 131.7, 129.6, 126.4, 126.1, 123.7, 122.3, 120.6, 116.6, 66.0, 32.9, 22.1. HR-ESIMS [M+Na] *m/z* calcd. for $C_{24}H_{21}N_3O_3Na$: 422.1481. Found: 422.1468. Δ = 3.1 ppm.

2-((1-(3,5-dichlorophenyl)-1H-1,2,3-triazol-4-yl)methoxy)-3-(3-metylbut-1-en-1-yl)naphthalene-1,4-dione (**16f**). Red solid, 60 % yield, m.p. 103-104 °C. IR (KBr, cm^{-1}) ν: 2666, 1660, 1646, 1585, 1557, 1477, 1251, 1184, 1037, 1001, 950, 915, 793, 723, 716, 666. ^{1}H NMR (DMSO-d_6, 500.00 MHz) δ ppm: 9.04 (1H, s), 8.04-8.03 (1H, m), 8.02 (2H, d, *J* 1.8 Hz), 8.01-7.98 (1H, m), 7.85-7.84 (2H, m), 7.72 (1H, t, *J* 1.8 Hz), 6.92 (1H, dd, *J* 7.1 and 16.3 Hz), 6.36 (1H, dd, *J* 1.5 and 16.3 Hz), 5.57 (2H, s), 2.38 (1H, ddq, *J* 1.5, 6.8 and 7.1 Hz), 0.95 (6H, d, *J* 6.8 Hz). ^{13}C NMR (DMSO-d_6, 125.0 MHz APT) δ ppm: 185.2, 181.4, 155.2, 150.5, 144.2, 137.1, 134.5, 134.2, 132.2, 131.7, 130.3, 139.6, 129.2, 126.4, 126,1. 123.4, 120.6, 120.5, 116.6, 66.1, 32.9, 22.1. HR-ESIMS [M+Na] *m/z* calcd. for $C_{24}H_{19}Cl_2N_3O_3Na$: 490.07016. Found: 490.0684. Δ = 6.5 ppm.

2-((1-(3-chlorophenyl)-1H-1,2,3-triazol-4-yl)methoxy)-3-(3-metylbut-1-en-1-yl)naphthalene-1,4-dione (**16g**). Red solid, 69 % yield, m.p. 107-108 °C. IR (KBr, cm^{-1}) ν: 3146, 2957, 2869, 1661, 1648, 1622, 1593, 1503, 1354, 1332, 1302, 1252, 1198, 1047, 962, 759, 721, 689. ^{1}H NMR (DMSO-d_6, 500.00 MHz) δ ppm: 8.96 (1H, s), 8.04-8.03 (1H, m), 8.01-7.98 (2H, m), 7.88 (1H, ddd, *J* 1.0, 2.1 and 8.1 Hz), 7.85-7.81 (2H, m), 6.73 (1H, t, *J* 8.1 Hz), 7.56 (1H, ddd, *J* 1.0, 2.0 and 8.1 Hz), 6.91 (1H, dd, *J* 7.0 and 16.3 Hz), 6.51 (1H, dd, *J* 1.4 and 16.3 Hz), 5.57 (2H, s), 2.37 (1H, ddq, *J* 1.4, 6.8 and 7.0 Hz), 0,94 (6H, d, *J* 6.8 Hz). ^{13}C NMR (DMSO-d_6, 125.0 MHz APT) δ ppm: 185.2, 181.3, 155.0, 150.6, 144.5, 138.6, 135.8, 134.6, 134.2, 132.2, 131.7, 129.6, 128.6, 126.4, 126.0, 123.8, 119.2, 116.6, 65.9, 32.9, 22.1. HR-ESIMS [M+H] *m/z* calcd. for $C_{24}H_{21}ClN_3O_3$: 434.1266. Found: 434.1268. Δ = 0.5 ppm.

2-allyl-3-((1-(4-chlorophenyl)-1H-1,2,3-triazol-4-yl)methoxy)naphthalene-1,4-dione (**17a**). Yellow solid, 57 % yield, m.p. 139-140 °C. IR (KBr, cm^{-1}) ν: 3132, 3095, 2958, 2918, 1670,1653, 1605, 1591, 1578, 1502, 1333, 1308, 1237, 1231, 1189, 1095, 1044, 991, 956, 930, 911, 830, 814, 797,725, 677, 652, 604. ^{1}H NMR (DMSO-d_6, 500.00 MHz) δ ppm: 8.96 (1H, s), 8.06-8.05 (1H,

m), 8.00-7.97 (1H, m), 7.94 (2H, d, *J* 8.9 Hz), 7.87-7.85 (2H, m), 7.67 (2H, d, *J* 8.9 Hz), 5.71 (1H, dddd, *J* 6.3, 6.3, 10.1 and 16.8 Hz), 5.86 (2H, s), 4.93 (1H, dd, *J* 1.7 and 16.8 Hz), 4.86 (1H, dd, *J* 1.7 and 10.1 Hz), 3.18 (2H, d, 16.8 Hz). ^{13}C NMR (DMSO-d_6, 125.0 MHz APT) δ ppm: 184.8, 181.4, 157.0, 144.3, 135.8, 134.7, 134.6, 134.3, 133.5, 133.4, 131.8, 131.7, 130.3, 126.5, 126.2, 123.6, 122.3, 116.6, 65.8, 27.9. HR-ESIMS [M+H] *m/z* calcd. for $C_{22}H_{17}ClN_3O_3$: 406.0953. Found: 406.0937. Δ = 3.9 ppm.

2-allyl-3-((1-(2,5-dichlorophenyl)-1H-1,2,3-triazol-4-yl)methoxy)naphthalene-1,4-dione (**17b**). Yellow solid, 59 % yield, m.p. 145-146 °C. IR (KBr, cm^{-1}) ν: 3164, 3094, 2968, 1669, 1651, 1615, 1593, 1578, 1486, 1452, 1334, 1264, 1228, 1186, 1153, 1043, 961, 899, 842, 722, 591, 573. ^{1}H NMR (DMSO-d_6, 500.00 MHz) δ ppm: 8.70 (1H, s), 8,06-8,04 (1H, m), 8.00-7.98 (1H, m), 7.88 (1H, d, *J* 2.5 Hz), 7.87-7.85 (2H, m), 7.79 (1H, d, *J* 8.7 Hz), 7.72 (1H, dd, *J* 2.5 and 8.7 Hz), 5.73 (1H, dddd, *J* 6.4, 6.4, 10.9 and 16.8 Hz), 5.60 (2H, s), 4.99 (1H, dd, *J* 1.6 and 16.8 Hz), 4.93 (1H, dd, *J* 1.6 and 10.9 Hz), 3.17 (2H, d, *J* 6.4 Hz). ^{13}C NMR (DMSO-d_6, 125.0 MHz APT) δ ppm: 184.7, 181.5, 157.0, 135.8, 134.6, 134.6, 134.2, 133.6, 133.6, 131.9, 131.8, 130.3, 126.4, 126.2, 123.5, 122.4, 116.5, 65.9, 27.9. HR-ESIMS [M+H] *m/z* calcd. for $C_{22}H_{15}Cl_2N_3O_3$:440.0490. Found: 440.0478. Δ = 2.7 ppm.

2-allyl-3-((1-(2-chlorophenyl)-1H-1,2,3-triazol-4-yl)methoxy)naphthalene-1,4-dione (**17c**). Yellow solid, 97 % yield, m.p. 62-63 °C. IR (KBr, cm^{-1}) ν: 3131, 3096, 1667, 1651, 1593, 1336, 1302, 1229, 1190, 1037, 954, 925, 802, 693. ^{1}H NMR (DMSO-d_6, 500.00 MHz) δ ppm: 8.61 (1H, s), 8.07-8.05 (1H, m), 8.00-7.98 (1H, m), 7.86-7.84 (2H, m), 7.74 (1H, dd, 1.6 and 7.8 hz), 7.65 (1H, dd, *J* 1.8 and 7.6 Hz), 7.62 (1H, td, *J* 1.8 and 7.8 Hz), 7.58 (1H, td, *J* 1.6 and 7.6 hz), 5.75 (1H, dddd, *J* 6.4, 6.4, 10.1 and 16.8 Hz), 5.62 (2H, s), 5.00 (1H, ddd, *J* 1.6, 3.4 and 16.8 Hz), 4.93 (1H, ddd, *J* 1.4, 3.4 and 10.1 Hz), 3.20 (2H, ddd, 1.4, 1.6 and 6.4 Hz). ^{13}C NMR (DMSO-d_6, 125.0 MHz APT) δ ppm: 184.0, 180.8, 156.2, 142.5, 133.9, 133.5, 128.1, 125.7, 125.5, 116.0, 65.1, 27.2. HR-ESIMS [M+H] *m/z* calcd. for $C_{22}H_{16}ClN_3O_3$: 406.0880. Found: 406.0857. Δ = 5.7 ppm.

2-allyl-3-((1-(3,4-dichlorophenyl)-1H-1,2,3-triazol-4-yl)methoxy)naphthalene-1,4-dione (**17d**). Yellow solid, 84 % yield, m.p. 104-105 °C. IR (KBr, cm^{-1}) ν: 3144, 3101, 2954, 1664, 1654, 1609,

1592, 1488, 1438, 1335, 1263, 1237, 1195, 1042, 1031, 959, 823, 814, 729. ^{1}H NMR (DMSO-d_6, 500.00 MHz) δ ppm: 8.97 (1H, s), 8.22 (1H, d, *J* 2.5 Hz), 8.07-8.05 (1H, m), 8.01-7.99 (1H, m), 7.94 (1H, dd, *J* 2.5 and 8.8 Hz), 7.87-7.85 (3H, m), 5.74 (1H, dddd, *J* 6.3, 6.3, 10.1 and 16.8 Hz), 4.96 (1H, dd, *J* 1.7 and 16.8 Hz), 4.89 (1H, dd, *J* 1.7 and 10.1 Hz), 5.58 (2H, s), 3.21 (2H, d, *J* 6.3 Hz). ^{13}C NMR (DMSO-d_6, 125.0 MHz APT) δ ppm: 184.7, 181.4, 156.9, 144.5, 136.5, 134.6, 134.6, 134.2, 133.6, 132.9, 132.2, 131.9, 131.7, 131.7, 162.4, 126.2, 123.7, 122.4, 120.7, 116.5, 65.9, 27.9. HR-ESIMS [M+H] *m/z* calcd. for $C_{22}H_{15}Cl_2N_3O_3$:440.0590. Found: 440.0562. Δ = 6.4 ppm.

2-((1-phenyl-1H-1,2,3-triazol-4-yl)methoxy)-3-(prop-1-en-1-yl)naphthalene-1,4-dione (**17e**). Yellow solid, 97 % yield, m.p. 129-130 °C. IR (KBr, cm^{-1}) ν: 3134, 3075, 1663, 1651, 1609, 1592, 1578, 1502, 1344, 1228, 1187, 1042, 949, 911, 901, 758, 724, 686, 649. ^{1}H NMR (DMSO-d_6, 500.00 MHz) δ ppm: 8.85 (1H, s), 8.07-8.06 (1H, m), 8.01-7.99 (1H, m), 7.88-7.85 (4H, m), 7.62-7.58 (2H, m), 7.52-7.48 (1H, m), 5.73 (1H, dddd, *J* 6.3, 6.3, 10.1 and 16.8 Hz), 5.59 (2H, s), 4.96 (1H, dd, *J* 1.7 and 16.8 Hz), 4.89 (1H, dd, *J* 1.7 and 10.1 Hz), 3.21 (2H, d, *J* 6.3 Hz). ^{13}C NMR (DMSO-d_6, 125.0 MHz APT) δ ppm: 184.8, 181.5, 157.0, 144.2, 137.1, 134.6, 134.6, 134.2, 133.6, 132.0, 131.8, 130.3, 129.2, 126.4, 126.2, 123.4, 120.7, 116.5, 66.0, 27.9. HR-ESIMS [M+H] *m/z* calcd. for $C_{22}H_{17}N_3O_3$: 372.1270. Found: 372.1242. Δ = 7.5 ppm.

2-allyl-3-((1-(3,5-dichlorophenyl)-1H-1,2,3-triazol-4-yl)methoxy)naphthalene-1,4-dione (**17f**). Yellow solid, 37 % yield, m.p. 101-103 °C. IR (KBr, cm^{-1}) ν: 3150, 3085, 2918, 1671, 1655, 1613, 1583, 1476, 1436, 1334, 1262, 1236, 1193, 1155, 1039, 960, 923, 853, 812, 802, 732, 665. ^{1}H NMR (DMSO-d_6, 500.00 MHz) δ ppm: 9.01 (1H, s), 8.07-8.05 (1H, m), 8.04 (2H, d, *J* 1.8 Hz), 8.01-7.99 (1H, m), 7.87-7.85 (2H, m), 7.71 (1H, t, *J* 1.8 Hz), 5.74 (1H, dddd, *J* 6.4, 6.4, 10.1 and 16.8 Hz), 5.58 (2H, s), 4.97 (1H, dd, *J* 1.7 and 16.8 Hz), 4.20 (1H, dd, *J* 1.7 and 10.1 Hz), 3.22 (2H, d, *J* 6.4 Hz). ^{13}C NMR (DMSO-d_6, 125.0 MHz APT) δ ppm: 184.7, 181.4, 156.9, 144.5, 138.7, 135.7, 134.7, 134.6, 134.2, 133.6, 132.0, 131.8, 128.5, 126.4, 126.2, 123.8, 119.3, 116.6, 65.8, 27.9. HR-ESIMS [M+H] *m/z* calcd. for $C_{22}H_{15}Cl_2N_3O_3$: 440.0490. Found: 440.0459. Δ = 7.0 ppm.

2-allyl-3-((1-(3-chlorophenyl)-1H-1,2,3-triazol-4-yl)methoxy)naphthalene-1,4-dione (**17g**). Yellow solid, 98 % yield, m.p. 104-105 °C. IR (KBr, cm^{-1}) ν: 3153, 3074, 2976, 1671, 1643, 1592, 1576, 1348, 1263, 1228, 1199, 1046, 1028, 954, 907, 791, 721, 685. ^{1}H NMR (DMSO-d_6, 500.00 MHz) δ ppm: 8.94 (1H, s), 8.07-8.05 (1H, m), 8.01-7.99 (2H, m), 7.89 (1H, ddd, *J* 1.0, 2.1 and 8.1 Hz), 7.87-7.88 (2H, m), 7.63 (1H, t, *J* 8.1 Hz), 7.55 (1H, ddd, *J* 1.0, 2.0 and 8.1 Hz), 5.74 (1H, dddd, *J* 6.3, 6.3, 10.1 and 16.8 Hz), 5.59 (2H, s), 4.96 (1H, dd, *J* 1.7 and 16.8 Hz), 4.89 (1H, dd, *J* 1.7 and 10.1 Hz), 3.21 (2H, d, *J* 6.3 Hz). ^{13}C NMR (DMSO-d_6, 125.0 MHz APT) δ ppm: 184.7, 181.5, 157.0, 144.4, 138.1, 134.7, 134.7, 134.2, 133.6, 132.0, 132.0, 131.8, 129.1, 126.4, 126.2, 123.6, 120.5, 119.3, 116.5, 65.9, 27.9. HR-ESIMS [M+H] *m/z* calcd. for $C_{22}H_{16}ClN_3O_3$: 406.0880. Found: 406.0853. Δ = 6.6 ppm.

2.2. Biological Assays

Cells and reagents. The human SCC-4, SCC-9 and SCC-25 cells, derived from a human oral tongue SCC, were obtained from ATCC (CRL-1624; CRL-1629 and CRL-1628, respectively) and maintained in 1:1 DMEM/F12 medium (Dulbecco's modified Eagle's medium and Ham's F12 medium; Gibco (Thermo Fisher, Waltham, MA, USA) supplemented with 10 % (v/v) FBS (fetal bovine serum; Invitrogen, Thermo Fisher, Waltham, MA, USA) and 400 ng/mL of hydrocortisone (Sigma-Aldrich Co., St. Louis, MO, USA). Primary normal human gingival fibroblast was obtained from ATCC (PCS-201-018) and maintained in DMEM supplemented with 10 % (v/v) FBS and were used at a maximum of 6 passages (4 passage for frozen stock vials and 2 passages for experimentation). Cells were cultured in a humidified environment containing 5 % CO_2 at 37 °C. For all biological experiments: Compounds were solubilized in 100 % DMSO (Sigma-Aldrich) to a final concentration of 10 mM. Carboplatin in water (Fauldcarbo®; Libbs Farmacêutica, São Paulo, SP, Brazil) was used as a standard anticancer compound.

Cell viability (Cytotoxicity) assay, compound stability assay. The SCC cell lines and primary human fibroblast cell metabolic activities (viability) were evaluated using the MTT assay. Cells were seeded in triplicate in 96-well plates (5 x 10^3 cells/well) and grown for two days until

confluence. Then, medium was removed, fresh medium was added, and the cells were returned to the incubator in the presence of different compounds. DMSO in the same concentrations was used as 100 % cell viability control. After 48 h, cells were incubated with 5 mg/mL MTT reagent (3-(4,5-dimethyl-2-thiazolyl)-2,5-diphenyl-2-*H*-tetrazolium bromide) (Sigma-Aldrich Co., St. Louis, MO, USA) for 3.5 h. Thereafter, the formazan crystals were dissolved in MTT solvent solution (DMSO/methanol 1:1 v/v), and the absorbance at 560 nm was evaluated using an EPOCH Microplate Spectrophotometer (BioTek Instruments, Winooski, VT, USA) with the background absorbance at 670 nm subtracted. Each of the 35 compounds was tested at six or seven different concentrations varying from 0.8 μM to 100 μM in cancer cell lines (SCC-4, SCC-9 and SCC-25) and 9.4 μM to 300 μM in primary normal human gingival fibroblast. Controls (carboplatin and lapachol) were tested at six or seven different concentrations varying from 31.20 μM to 1,000 μM in cells. Compounds that did not reach the IC_{50} between this concentration threshold were considered Not Determined (ND). For the assays using inhibitors of caspases, SCC-9 cells were incubated with ZVAD or ZDEVD (Sigma-Aldrich Co., St. Louis, MO, USA) at 20 μM for 2 h and then treated with 1xIC_{50} of compound **16g** or control (DMSO) for more 24 h. MTT assay was then carried as described above.

Hemolysis assay. The hemolysis evaluation of derivatives was performed using fresh lamb blood from CECAL/FIOCRUZ (breeding center of laboratory animals). Erythrocytes were collected by centrifugation at 1500 rpm for 15 min., washed three times with phosphate-buffered saline (PBS) with 10 mM glucose at pH 7.4 and counted in a Countess® FLII Automated Cell Counter (Thermo Fisher, Waltham, MA, USA). Erythrocytes were seeded in 96-well plates at a concentration of 4 x 10^8 cells/well in triplicate, and 10 μL of the compounds was added at a final concentration of 400 μM in glucose-PBS (100 μL final volume). Ten microliters of PBS were used as a negative control (0 % hemolysis), and 10 μL of PBS with 0.1 % Triton X-100 was used as a positive control (100 % hemolysis). The solutions were mixed and incubated in a shaker for 30 min. at room temperature. After centrifugation at 13,000 rpm for 15 min., hemolysis was measured by reading the supernatant absorbance at 540 nm on an EPOCH Microplate Spectrophotometer (BioTek Instruments, Winooski, VT, USA). All hemolysis data points were presented as the percentage of the complete hemolysis control.

Clonogenic assay. The ability of individual SCC9 and normal fibroblasts cells to undergo "unlimited" division was tested using a clonogenic assay. Cells were seeded in duplicates in 24-well plates (5 x 10^3 cells/wells) for 24 h. Fresh medium was added in the presence of the indicated compounds at the concentrations of 1x IC_{50} and 2x IC_{50} as determined for SCC-9 cells. DMSO at the same concentrations of the compounds was used as a 100 % control. On the fifth day (120 h), the wells were fixed with ethanol for 10 min., followed by staining with 0.05 % crystal violet (Sigma-Aldrich) in 20 % ethanol for 10 min and washed three times with distilled water and set to dry. Wells were photographed and the absorbance was read in spectrophotometer at the 595 nm microplate spectrophotometer (EPOCH, BioTek Instruments, Winooski, VT, USA), after solubilization of the dye in 33 % acetic acid.

In vivo acute toxicity study. Acute toxicity study for the compound was conducted in twelve weeks old female C57BL/6 mice through intraperitoneal injection route and was approved by the University animal ethical council under de registration number 982. All experiments were performed in accordance with Brazilian guidelines and regulations. Dosing and analysis were done as per OECD 423 guidelines and as reviewed by Parasuraman [34]. Each animal group had n = 3 and received only one intraperitoneal injection (Day 0) of each compound dissolved in 3 mL of PBS and 3 % of DMSO. Control animals received only 3 % of DMSO in PBS. The first dose of the compound was 50 mg/kg. Subsequent dose levels (150 mg/kg and 450 mg/kg) were determined based on the result after the previous dosing. Animals were examined every day, two times a day for mortality and morbidity for 14 days, when all animals were anesthetized (ketamine 100 mg/kg and xylazine 10 mg/kg) and euthanized by cervical dislocation and gross necropsy and major organs histology was accessed. Animal body weight and average food consumption were measured every 7 days. As morbidity indication, the following signs were accessed two times a day: tremors; convulsion; salivation; diarrhea; lethargy; coma; signs of pain; increased back arching and mobility defect. The necropsy included an examination of the external features of the carcass; external body orifices; the abdominal, thoracic, and cranial cavities; organs/tissues of liver, thymus, right kidney, right testicle, heart, and lung. For more details, see Supplementary Methods (Appendix A).

Videomicroscopy. SCC-9 cells, previously plated the day before the experiment, were treated and transferred to a culture chamber adapted to a Nikon Eclipse TE300 microscope (Nikon, USA) under controlled conditions of CO_2 and temperature (5 % and 37 °C, respectively). For 24 hours, phase contrast images from the same field were captured every minute using a Hamamatsu C2400 CCD camera (Hamamatsu, Japan). Two experimental conditions were performed: control (DMSO) and treatment with **16g** compound (2 x IC_{50}). Images of each experimental condition were integrated in videos using the ImageJ software (National Institute of Health, USA).

Immunocytochemistry. SCC-9 cells, previously plated the day before the experiment in round 13 mm coverslips, were treated as described above for 4 and 24 h. Then, they were fixed for 15 min. with PBS-paraformaldehyde 4 %, treated with PBS-triton X100 0.2 % for 5 min., blocked with PBS-BSA 5 % (Sigma-Aldrich, USA) for 30 min. and incubated overnight with α-tubulin (Sigma-Aldrich, USA) or LC3 (Cell Signaling; ab48394) primary antibody. Then, secondary monoclonal Alexa 546 nm antibody (Molecular Probes Inc, USA) was incubated for 2 h as the fluorescent probes. Finally, cells were incubated for 10min with DAPI, and coverslips were mounted in glass slides to be visualized using a Leica TCS-SP5 II confocal microscope (Leica Microsystems, Germany). Confocal fluorescence images were captured employing the LAS AF 2.2.0 Software (Leica Microsystems, Germany).

For cleaved caspase-3 analysis, cells were plated on coverslips placed on a 24-well plate. After 30 min. of compound incubation at a concentration of 2 x IC_{50}, the cells were fixed with 4 % paraformaldehyde in phosphate buffer for 15 min. The fixed cells were then washed with PBS and incubated with 5 % bovine serum albumin (BSA) diluted in PBS for 60 min. After this, the cells were incubated overnight at 4 °C with a Cleaved Caspase-3 Antibody (Alexa Fluor® 488 Conjugate) (1:50 dilution; Cell Signaling; #9669). Then, were washed with PBS, stained with DAPI, washed again and mounted. The cells were imaged using an inverted fluorescence Zeiss Axio Observer microscope.

ROS Production. Dihydrorhodamine 123 is used for the detection of ROS (reactive oxygen species). The presence of ROS oxidizes the dihydrorhodamine 123 to the fluorescent derivative rhodamine 123. To verify the level of mitochondrial ROS by fluorescence microscopy, 5 x 10^4 cells per well were plated on a 24-well plate. After 6 hours of compounds incubation at a

concentration of 2 x IC_{50}, DHR123 (Sigma; # D1054) was added at a final concentration of 1.2 μM for 15 min. at 37 °C and then washed twice with medium. Cells were analyzed using an inverted fluorescence Zeiss Axio Observer microscope.

Molecular modeling analysis. The most active compound (**16g**) was submitted to docking studies in attempt to provide a possible mechanism of action of these derivatives. The binding mode and interactions were compared with lapachol and other inhibitors of lapachol targets. Ligands and receptors were prepared for the docking studies. The three-dimensional structures of the lapachol and the derivative **16g** were constructed using Spartan'10 program (Wavefunction Inc. Irvine, CA, USA). Initially, structures were submitted to a conformational analysis using molecular mechanics and the MMFF force field. Then, the geometry of the lowest-energy conformer was optimized in a vacuum by the semi-empirical method RM1, followed by a single point calculation using the density functional theory (DFT) method with B3LYP/6-31G* basis set. Electrostatic charges were added and torsions of ligands were set automatically using Autodock Tools 1.5.7. The structures of DNA-binding domain of human topoisomerase I, topoisomerase IIα and topoisomerase IIβ were retrieved from Protein Data Bank (PDB) under the codes 1K4T [23], 5GWK [24] and 3QX3 [25], respectively. Meanwhile, the structure of human pyruvate kinase M2 (hPKM2) complexed with oxalate and fructose-1,6-biphosphate was obtained from PDB with the code 3SRD. Molecular docking studies were carried out using Autodock Tools 1.5.7 and Autodock Vina 1.1.2 [26]. Initially, solvent and ligands were removed from protein structures. Polar hydrogens and Gasteiger charges were added to protein structures. To evaluate the binding mode of compounds against topoisomerases, we employed docking protocols validated previously by our group and described elsewhere [27]. To validate the docking method of pyruvate kinase, the redocking of ATP was carried out in the active site of rabbit muscle pyruvate kinase (PDB code 1A49) [28]. The grid box with dimensions of 18 x 24 x 20 $Å^3$ was centered on residue H77 (H78 in hPKM2). The search parameters were kept as default, except for the exhaustiveness that was set to 5. Finally, the lowest-binding-energies of the conformers (Kcal/mol) were evaluated and conformer was the one with the lowest value for each ligand was selected for visual inspection and the binding mode analysis were carried out. Finally, the conformers with the lowest binding energy were selected for visual inspection and the binding mode analysis were carried out using Pymol v. 1.2r2 (The PyMOL Molecular Graphics System, Version 1.2r2 Schrödinger, LLC).

Statistical analysis, IC50 calculation. The IC_{50} values for the MTT assay were obtained by nonlinear regression using the GRAPHPAD 5.0 program (Intuitive Software for Science, San Diego, CA) from at least 3 independent experiments. Data are presented as means ± S.D. A dose-response log (inhibitor) vs. response curve using fitting least squares method was used to determine the IC_{50}, SD and R^2 of the data. Selective index was calculated as S.I. = IC_{50} of compound in normal oral fibroblasts cells/IC_{50} of the same compound for each oral cancer cell line (SCC-4, SCC-9 and SCC-25) and the average was calculated when indicated.

3. Results and discussion

3.1. Chemistry

Initially, we performed the synthesis of *O*-propargyl quinones **6-10** using a sequence of reactions that involved C-3 alkylation by Knoevenagel condensation (to obtain **2-4**) [14-17] or [3.3]-sigmatropic rearrangement (to obtain **5**) [18]. Then, the treatment of quinones 2-5 with propargyl bromide refluxing acetone and K_2CO_3 led to the propargylated quinones **6-10** in 50-84 % yields [19, 20]. On the other hand, arylazides **12a-g** were prepared, in quantitative yields, from commercial anilines through their treatment with sodium nitrite in hydrochloric acid at 0-5 ºC followed by aromatic electrophilic substitution with sodium azide (Scheme 1) [21, 22].

Finally, the reaction between the arylazides **12a-g** and *O*-propargyl quinones, **6-10** catalyzed by Cu(I), provided only the 1,4-disubstituted regioisomer from the protocol based on a Huisgen 1,3-dipolar cycloaddition CuAAC in 30-97 % yields (**Fig. 1**).

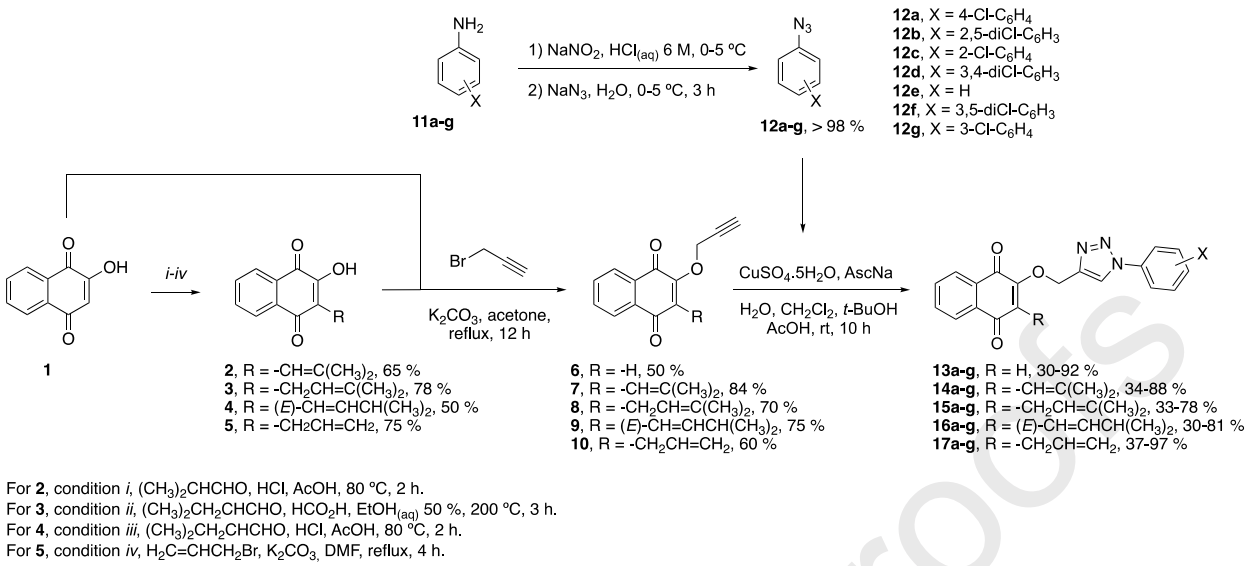

Fig. 1. Synthesis of 1,4-naphthoquinones tethered to 1,2,3-1*H*-triazoles **13-17**

The structures of the compounds were elucidated by spectroscopic techniques (see Experimental Section and Supplementary Information). For example, the ^{1}H NMR spectrum analysis of compound **16g** (highlighted compound derived from isolapachol), it could be observed a singlet at 5.57 ppm corresponding to OCH_2 tethered to 1,2,3-triazole ring; it could be observed doublet of doublet of quartets at 2.37 (ddq, *J* 1.4, 6.8 and 7.0 Hz) corresponding to $C\underline{H}(CH_3)_2$ protons of C-3 side chain; it was also observed a the typical benzoaromatic pattern of 1,4-naphthoquinone isomers as multiplets at 8.01-7.98 and 7.85-7.81. Moreover, in the aromatic region, the singlet at 9.04 ppm assigned to the resonance of the proton resonance of triazolic ring CH.

3.2. Evaluation of biological activity

Human OSCC cell lines survival, Selective Index, Hemolytic activity and Compounds stability

All thirty-five new compounds were first screened by the sensitive cell viability MTT assay. This assay is a colorimetric analysis that quantifies total viable cells indirectly based on the conversion of MTT salt from yellow to purple due to formazan formation. It is a classical assay to determine the cytotoxicity of anticancer compounds and was used to investigate the application of

these compounds as target drugs. In order to select highly active compounds, cytotoxic activity was first tested in a single human tongue squamous cell carcinoma (SCC-9) cell line with a maximum concentration threshold of 100 μM and compounds with IC_{50} higher than this concentration were considered Not determined (ND), as previously characterized [6, 29]. Furthermore, higher concentration then 100 μM of several new compounds tend to be insoluble in medium generating misleading results. Carboplatin, a widely used chemotherapeutic agent for this type of cancer, and lapachol, a similar naphthoquinone with a natural origin extracted from *Tecoma* trees or from synthetic sources that has pronounced anticancer activity [7], were used as positive controls. Regression curves were calculated and used to determine IC_{50}. Among all thirty-five compounds, seventeen achieved 50 % of viability reduction in the tested concentrations threshold (0.8-100 μM) (**Table 1**). Anticancer activities of these compounds are reported here for the first time.

Table 1. Determination of IC_{50} and Selective Index of the new synthesized triazole naphthoquinones. SCC-9 (OSCC cells) or normal human gingival fibroblast were treated with the indicated compound for 48 h and cell viability was determined as indicated in material and methods. It is shown from left to right: compound structure, name, SCC-9 tumor or normal fibroblast IC_{50} (μM), SD and Selective index (SI) of at least 3 independent experiments. SI = IC_{50} of compound in normal oral fibroblasts cells / IC_{50} of the same compound for SCC-9 oral cancer cell line. SD = standard deviation; ND = not determined (compounds with IC_{50} above the tested concentration threshold of 100μM)

Compounds	SCC-9 Oral		Primary Gingival Fibroblast		Selective Index (SI)
	IC_{50}	SD	IC_{50}	SD	
13a	ND	ND	ND	ND	ND
13b	ND	ND	ND	ND	ND
13c	69.33	0.15	32.54	0.07	0.47
13d	29.04	0.14	43.08	0.47	1.48
13e	44.41	0.10	11.80	0.20	0.27
13f	61.50	0.08	102.10	0.23	1.66
13g	56.13	0.09	54.10	0.38	0.96
14a	35.48	0.31	47.59	0.19	1.34
14b	31.48	0.08	45.94	0.06	1.11
14c	27.89	0.35	34.87	0.05	1.25

14d	33.11	0.32	60.38	0.01	1.82
14e	60.19	0.38	59.52	0.00	0.99
14f	71.31	0.32	34.33	0.09	0.48
14g	77.99	0.25	49.30	0.05	0.63
15a	ND	ND	ND	ND	ND
15b	ND	ND	ND	ND	ND
15c	ND	ND	ND	ND	ND
15d	ND	ND	ND	ND	ND
15e	ND	ND	ND	ND	ND
15f	ND	ND	ND	ND	ND
15g	ND	ND	ND	ND	ND
16a	33.88	0.24	70.45	0.35	2.08
16b	79.43	0.32	173.20	0.19	2.18
16c	ND	ND	ND	ND	ND
16d	ND	ND	ND	ND	ND
16e	33.07	0.08	62.40	0.10	1.89
16f	N.D.	N.D.	N.D.	N.D.	N.D.
16g	66.06	0.34	209.90	0.16	3.18
17a	ND	ND	ND	ND	ND
17b	ND	ND	ND	ND	ND
17c	89.07	0.37	114.20	0.17	1.28
17d	ND	ND	ND	ND	ND
17e	ND	ND	ND	ND	ND
17f	ND	ND	ND	ND	ND
17g	ND	ND	ND	ND	ND
Carboplatin	268.3	0.03	394.1	0.04	1.46
Lapachol (**3**)	108.04	0.11	296.90	0.02	2.75
Doxorubicin	7.2	0.04	18.68	0.07	2.57

The degree of selectivity of these compounds can be expressed by their Selective Index (SI). A high SI value ≥ 2 of a compound represents a selective toxicity towards cancer cells, while a SI value < 2 is considered generally toxic, such that it can also cause cytotoxicity in normal cells [6, 30-32]. Accordingly, each SI value was calculated using the given formula: SI = IC_{50} normal cell / IC_{50} cancer cell. A primary non-transformed gingival human fibroblast (normal cell) was used to determine the SI of tested compounds. Comparison between the IC_{50} in normal cells and SCC9 cell line and calculation of the SI demonstrates that only compounds **16a**, **16b** and **16g** displayed a SI higher than 2 (SI **16a** = 2.08, SI **16b** = 2.18, SI **16g** = 3.18) as shown in Table 1. All other compounds and, surprisingly, carboplatin showed SI < 2. Lapachol and doxorubicin were also selective in SCC-9 cells with a SI of 2.74 and 2.57, respectively.

Initial screening was performed exclusively in SCC-9, as it exhibits the most stringent phenotype (lower sensitivity) to cytotoxic agents of the different SCC cell lines, as previously demonstrated [6, 29]. To limit possible aberrations in behavior from a single cell line when compared with cancer cells in patients and to determine the effectiveness of these compounds against oral cell carcinoma, the three selective compounds were tested in two other oral human carcinoma cell lines, SCC-4 and SCC-25. These cell lines were, as expected, even more susceptible to compounds **16a**, **16b** and **16g**, leading to an average SI of 2.40 for **16a**, 3.55 for **16b** and 6.01 for **16g** (**Table 2**). Carboplatin maintained its SI below 2 and surprisingly average SI for Lapachol (**3**) decreased to 1.56, suggesting that these compounds are less selective than the new tested compounds. Only doxorubicin (SI = 3.39) had a SI > 2. Taken together, the above results demonstrated that compounds **16a**, **16b** and **16g** were able to induce cytotoxicity in three different cell lines of human oral squamous cell carcinoma and were more or comparably toxic and selective to tumor cells than classical and chemically similar controls.

Table 2. Characterization of the most selective compounds in other OSCC cells and analysis of colony formation and hemolytic activity. The IC_{50} (μM) of three different OSCC cell lines (SCC-4, SCC-9 and SCC-25) and normal fibroblast cells followed by the average selective index of compounds **16a**, **16b** and **16g** was calculated as in Table 1. All experiments are results of at least 3 independent experiments.

Compounds	Oral Tumor Cells						Average IC_{50}	Primary Gingival Fibroblast		Average SI
	SCC-4		SCC-9		SCC-25					
	IC_{50}	SD	IC_{50}	SD	IC_{50}	SD		IC_{50}	SD	
16a	36.30	0.37	33.88	0.24	18.19	0.27	29.46	70.45	0.35	2.40
16b	43.65	0.31	79.43	0.32	23.44	0.39	48.84	173.20	0.19	3.55
16g	28.84	0.25	66.06	0.34	9.81	0.18	34.90	209.90	0.16	6.01
Carboplatin	316.70	0.52	268.3	0.03	270.80	0.46	266.90	394.10	0.04	1.37
Lapachol (**3**)	218.3	0.01	108.04	0.11	237.1	0.07	187.48	296.90	0.02	1.58
Doxorubicin	5.87	0.13	7.26	0.04	3.37	0.05	5.5	18.16	0.07	3.39

After initial screening, the three compounds selected through cytotoxicity assays were tested by the highly sensitive clonogenic assay, which is an *in vitro* cell survival assay based on the ability of a single cell to grow into a colony. The assay essentially tests every cell in the population for its ability to undergo "unlimited" division. Clonogenic assay is the method of choice

to determine cell reproductive and death and is used to determine the effectiveness of cytotoxic agents [33]. Colony formation and densitometry were accessed five days after treatment with variable concentrations of the compounds.

The three compounds (**16a**, **16b** and **16g**) significantly reduced colony formation of SCC-9 cell line in the tested concentrations with variable potencies (**Fig. 2A**). To enable the analyses and comparison of phenotype induced between each compound we used a normalized IC_{50} dose calculated for SCC-9 cells for these experiments (2 times the IC_{50}). It is remarkable that compounds **16a** and **16g** exhibited similar cytotoxicity to chemotherapy drug carboplatin in reducing colony formation. Also, it is outstanding that the reduction in colony formation was more prominent in SCC-9 cells than in normal cells, showing again the selectivity of these compounds (**Fig. 2A**). Altogether, these results suggest that compounds **16a**, **16b** and **16g** may become promising targets for further analysis.

Furthermore, to discard any surfactant activity of the compounds, which could lead to unspecific cytotoxicity through cellular membrane damage, a hemolytic assay was performed. Compounds **16a**, **16b** and **16g** were evaluated at a concentration of 400 μM, approximately 10 times the average IC_{50} of these compounds in cancer cells. No compound exhibited hemolysis higher than 5 %, a level that is comparable to carboplatin and that of the solvent alone (DMSO; **Fig. 2B**).

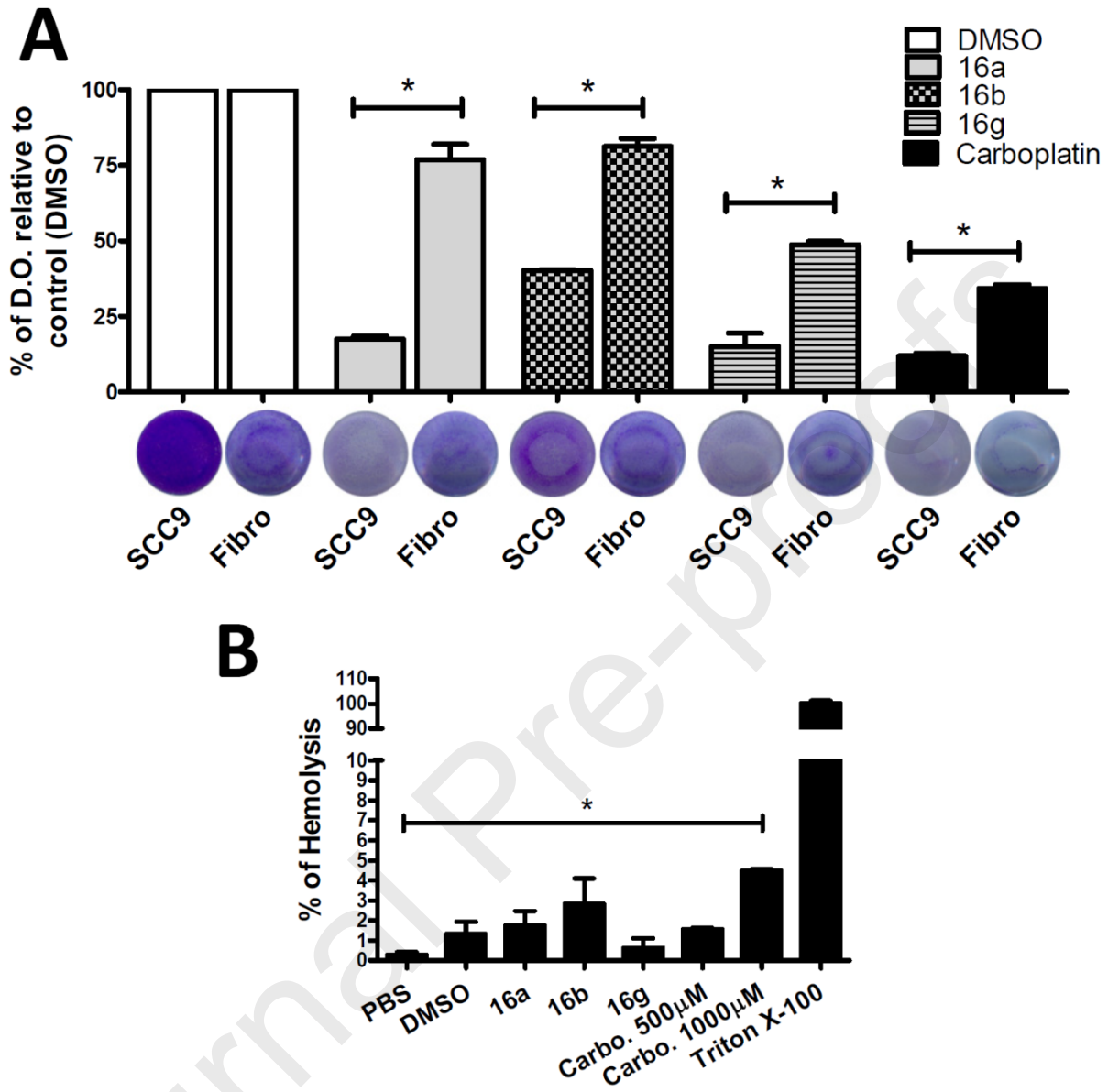

Fig. 2. (A) Clonogenic assay: each column indicates the cell type (SCC-9 or normal fibroblast) treated with indicated compound. Cells were treated with two times of the calculated IC_{50} (2 x IC_{50}) in SCC-9 cells (**16a**: 67.76 µM; **16b**: 87.34 µM; **16g**: 132.12 µM). The use of the normalized concentration with the IC_{50} is useful to analyze the effect between each compound. Top: graphical analyses of colony formation by absorbance reading as indicated in material and methods. Bottom: representative wells of colony formation assay stained with crystal violet. One-way ANOVA with Boferroni´s Multiple Comparation post test was performed where all columns were significantly different from control (DMSO) and * represents $p < 0.0001$. (B) Hemolytic activity of compounds at 400 µM (approximately 10 x IC_{50}). One-way ANOVA with Dunnett post test was performed

where all columns were significantly different from control (Triton X) with $p < 0.0001$. All experiments are results of at least 3 independent experiments.

In vivo acute toxicity study

Preclinical animal studies were performed as additional tests with compounds **16a**, **16b** and **16g** for future clinically applicable drugs. Due to cytotoxicity activity data which revealed that these compounds are more effective (low IC_{50} versus high SI) than other tested compounds it was decided to assay their acute toxicity. Toxicity testing of new compounds is essential for drug development process. The preclinical toxicity testing on various biological systems reveals the species-, organ- and dose- specific toxic effects of an investigational product. Toxicological screening is very important for the development of new drugs and for the extension of the therapeutic potential of existing molecules. The US Food and Drug Administration (FDA) states that it is essential to screen new molecules for pharmacological activity and toxicity potential in animals (21CFR Part 314). Acute toxicity testing was carried out to determine the effect of a single dose on a particular animal species [34].

For the acute toxicological testing, the three compounds were administered intraperitoneally in C56BL/6 mice at different concentrations and their effect was observed along 14 days. All mortalities caused by the compounds during the experimental period were recorded and morphological, pathological, and histological changes in the dead animals were investigated. A sequential procedure in which three animals of the same sex were used in each step was done as follow: a single dose of a lower concentration of 50 mg/kg was used. Since there was no indication of morbidity and less than 2 causalities, the next group received a concentration of 150 mg/kg and for the same reason a third group received a concentration of 450 mg/kg (**Table 3**, Supplementary **Table S1** and Supplementary **Fig. S1**). No significant alteration in body weight and food consumption relative to control animals in any concentration of tested compounds was observed (**Table 3** and Supplementary **Fig. S1A** and **S1B**). Furthermore, no alteration in morbidity was observed (**Table 3**). The death of one animal was observed only in the group treated with compound **16b** at 150 mg/kg but since it didn't achieve 50 % of the animals in the group we proceeded to a higher dose (450 mg/kg) to try to determine the LC_{50}. However, no lethality was observed at this higher dose. Regarding gross major organs necropsy, it was noticed an *in loco* precipitation of compound **16a**, at 150 and 450 mg/kg (**Table 3**). In the histopathological analysis,

the effect of a mild binucleation and megalocytosis, an indication of moderate degree of hepatic cellular stress of hepatocytes, were observed only in groups that received 450 mg/kg of all tested compounds. Binucleation is a normal phenomenon of a healthy liver but may be involved with liver recovery after injury and is a characteristic of liver regeneration. The presence of binucleation and megalocytosis in the absence of necrotic or inflammatory processes suggests that a discrete hepatic damage may be related to oxidative stress induced by the high dose of compounds. However, animals of group treated with 450 mg/kg of **16a** showed findings that were not present in any other group; they presented peritoneal nodules with lesion pattern compatible with immune granuloma, which may be associated with the reaction to the inoculated substance. Taken together, the results obtained from this experiment demonstrated no apparent limiting toxic effects of compound **16g** on mice in the tested concentrations, making this compound a good candidate for further anticancer *in vivo* tests. On the other hand, compounds **16a**, which was not fully absorbed and induced immune granuloma, and **16b**, that lead to one lethality in the tested concentrations but did not reach LC_{50}, are less promising candidates.

Table 3. Acute toxicity study: Morbidity, mortality, gross organs necropsy and histology of mice treated with compounds **16a**, **16b** and **16g**.

Treatment	Dose mg/Kg[a]	Change in body weight	Change in food consumption	Morbidity[b]	Mortality	Gross Necropsy[c]	Histology[d]
Control	0	Absent	Absent	Absent	Absent	No alteration	Normal
16a	50	Absent	Absent	Absent	Absent	Precipitated	Normal

	150	Absent	Absent	Absent	Absent	compound *in loco* Precipitated compound *in loco*	Normal
	450	Absent	Absent	Absent	Absent	No alteration	Peritoneal Immune granulomas; Moderate megalocytosis; Moderate hepatocyte Binucleation;
16b	50	Absent	Absent	Absent	Absent	No alteration	Normal
	150	Absent	Absent	Absent	1 death	No alteration	Normal
	450	Absent	Absent	Absent	Absent	No alteration	Moderate megalocytosis; Moderate hepatocyte Binucleation
16g	50	Absent	Absent	Absent	Absent	No alteration	Normal
	150	Absent	Absent	Absent	Absent	No alteration	Normal
	450	Absent	Absent	Absent	Absent	No alteration	Moderate megalocytosis; Moderate hepatocyte Binucleation

[a]Dose level for each subsequent group was determined based on the result after the previous lower dosing. [b]Morbidity symptoms were analyzed every day, two times a day and were considered as: Tremors; Convulsion; Salivation; Diarrhea; Lethargy; Coma; Signs of Pain; Mobility defect. [c]Gross organ necropsy of liver, thymus, right kidney, right testicle, heart, major lymph nodes and lung. [d]Histopathology of the lung, kidney, heart, liver and spleen was accessed by trained pathologist and are summarized here. For more information and results see Supplementary Table S1.

Investigation of cell death mechanisms

In view of the results showing high cytotoxicity (~ 35μM), selectivity (SI ~ 6) and low acute toxicity on animals, we decided to deepen our studies exclusively on compound **16g**. Then, we aimed to investigate cell death molecular mechanisms triggered by compound **16g** treatment. Chemotherapeutic agents are well-known to induce cell death by boosting reactive oxygen species (ROS) production, directly binding to DNA by intercalation or between double helix grooves, by promoting microtubule disorganization and inhibiting topoisomerases activity. All these molecular mechanisms were explored for the **16g** compound.

ROS Production

The production of ROS was assessed using DHR123, a cell-permeable fluorogenic probe and an indicator of ROS levels, after 6 hours of compound **16g** incubation. There was a low production of ROS on SCC-9 cells, similar to solvent alone (DMSO), but significantly different of positive control (H_2O_2) (Supplementary **Fig. S2**), demonstrating that ROS production is not triggered by compound **16g**. Latter times (12 h and 24 h) were also accessed with similar results (data not shown).

DNA Binding

We next investigated a possible interaction between compound **16g** with DNA by calorimetry (Supplementary **Fig. S3**). Doxorubicin was used as a positive control since it was characterized to interact with DNA [35] and the calorimetric traces can be observed in Supplementary **Fig. S3B**. The Q/mol changes as a function of the concentration of poly(GC) DNA, confirming Doxorubicin-DNA interaction in a process enthalpically driven at 37 °C. On the other hand, the small difference among the heat of dilution of poly(GC) DNA in buffer and the heat released in **16G** solution (Supplementary **Fig. S3A**) can be associated to absence of residual DMSO in the buffer, indicating no binding or a very low-affinity binding of this compound.

Microtubule organization

Still seeking for a molecular mechanism of cell death that could explain compound **16g** toxicity, we further analyzed the microtubule of cells in a determined time point. Through immunocytochemistry, it was possible to note that compound **16g** (2 x IC_{50}) induced an increase in tubulin filaments disorganization after 4h of treatment followed by a complete disruption of the network after 24 h of treatment (**Fig. 3**), thus, showing that treatment with compound **16g** is able to induce microtubule disarrangement.

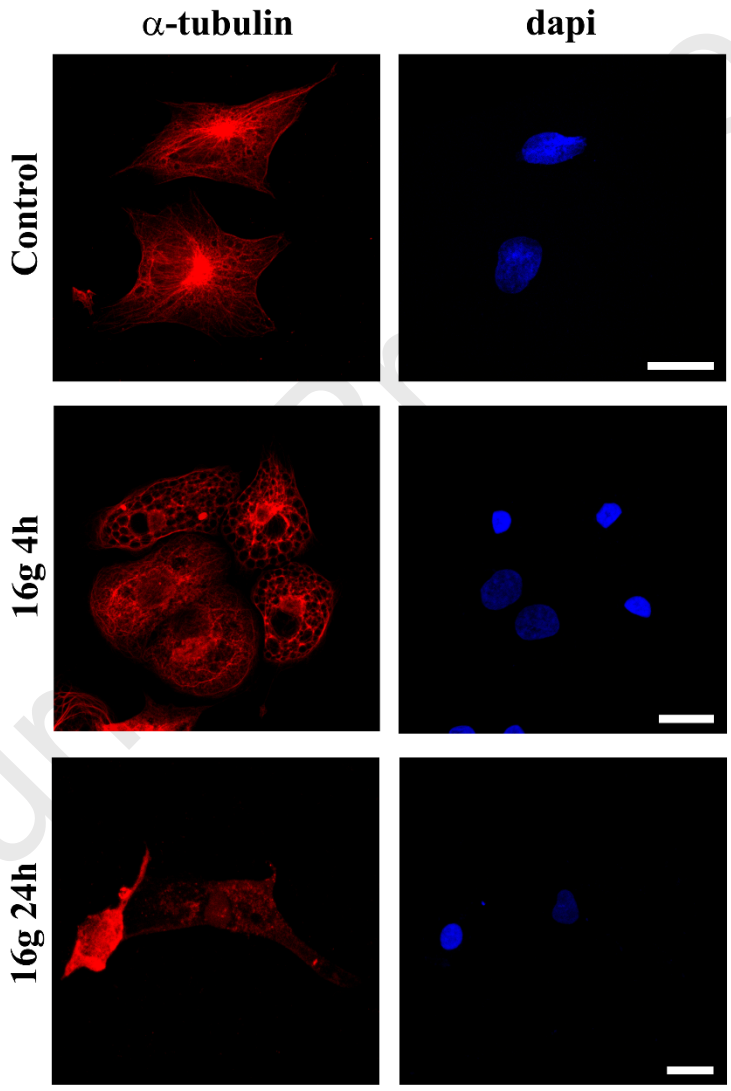

Fig. 3. Compound **16g** induces microtubules disorganization. Representative confocal fluorescence images of tubulin filaments of SCC9 cells revealed that **16g** treatment (2 x IC_{50}) induced an increase in filaments disorganization after 4h followed by a complete disruption of the

network after 24h. Images were selected as the representative results of at least 3 independent experiments. Scale bars are all 20μm.

Microtubules have critical functions in cell survival, acting on cellular organization, cargo transport and chromosome segregation during mitosis [36]. Indeed, several chemotherapeutic agents used in clinic target microtubules, such as the well-known Taxol, Vinblastine and Vincristine [37].

Molecular docking of compound 16g

To investigate a possible mechanism of action of **16g**, we searched for other similar compounds with well-known mechanisms of cell death and established a y molecular modeling analysis.

As mentioned before, lapachol was used as a control in the cytotoxic assays for being as it is a similar naphthoquinone similar to our compounds, with pronounced anticancer activity. Indeed, the antitumoral activity of lapachol and its derivatives has been widely explored in many human cell lines and one of the mechanisms of action identified so far is the inhibition of DNA topoisomerase enzymes [38-41]. Thereby, to investigate the possible molecular mechanism of antitumor activity of compound **16g**, we docked it as well as lapachol with DNA topoisomerase I, IIα and IIβ and compared their binding mode with the ones of known inhibitors of these enzymes. In this session the results will shortly be presented; the detailed analysis of compound **16g** and its possible targets can be found at supplementary material.

The naphthoquinone derivative **16g** showed a different binding mode to topoisomerase I, compared to lapachol (**3**). The binding energy of the complex of **16g** (-10.7 Kcal/mol) with topoisomerase I was similar to that of topotecan (-11.5 Kcal/mol), a known inhibitor of this enzyme, and lower than that of lapachol (**3**, -8.4 Kcal/mol). Compound **16g** also exhibited a different binding mode to topoisomerase IIα comparing with lapachol (**3**). The binding energy found in the docking of **16g** with topoisomerase IIα was -10.3 Kcal/mol, which was higher than that of etoposide (-13.1 Kcal/mol), known topoisomerase II inhibitor, and lower than that of lapachol (-8.2 Kcal/mol). Also, in the case of topoisomerase IIβ, the binding energy of **16g** (-11.0

Kcal/mol) was higher than etoposide (-14.7 Kcal/mol) but lower than lapachol (**3**, -8.9 Kcal/mol) (**Fig. 4A-C**).

Our results showed that lapachol can intercalate with DNA complexed with topoisomerase enzymes theoretically which is in agreement with several experimental data [35-38]. Quinone ring of **16g** did not superpose to the quinone of lapachol (**3**), only in the case of topoisomerase IIβ, they were positioned in the same region. It is probably due to the greater size of **16g** in comparison to lapachol and the presence of the aromatic rings (phenyl and triazole), which superposed with the rings of the known inhibitors. However, but compound **16g** seems to resemble the binding manner and interaction network of known inhibitors of the studied topoisomerases, suggesting these enzymes could be potential targets for the anticancer action of this compound.

Topoisomerase enzymes preserve DNA topology throughout replication and transcription, and is also being essential for cell survival. Inhibitors of topoisomerases, such as Etoposide, Topotecan and Irinotecan, are similarly indispensable to fight cancer in the clinic [42]. All these drugs present at some extent dose limited toxicities and/or the development of resistance [37, 42]. In this context, compound **16g** emerges as a possible future choice of cancer treatment targeting microtubules and/or topoisomerases and could be combined with other anticancer drugs for a better outcome.

Recently, it was demonstrated that lapachol inhibits hPKM2 enzyme involved in the glycolysis pathway and further impairs cancer cell metabolism which can contribute to its antitumoral activity [43]. Hence, we also investigated this enzyme as a potential biological target for **16g**. First, we validated our docking protocol by redocking ATP within the active site of the rabbit muscle pyruvate kinase (Supplementary material). Lapachol bound at the entrance of the active site like the adenine group of ATP in the active site of the homologous enzyme [28]. Compound **16g** exhibited a similar binding mode. The binding energy of the complex of **16g** with hPKM2 was -8.1 Kcal/mol. This value is in the range of those found for the redocking of ATP (-9.4 Kcal/mol) and for the docking of lapachol (-6.8 Kcal/mol) (**Fig. 4D-G**), suggesting that inhibition of hPKM2 may be also a feasible mechanism of action for the antitumoral profile of **16g**.

Altogether these data suggest that compound **16g** may bind with higher affinity (lower binding energy) than lapachol and with affinity close to current anticancer drugs to topoisomerase

I, II (α and β) and hPKM2. All these modes of action could be responsible for cell death induction observed above.

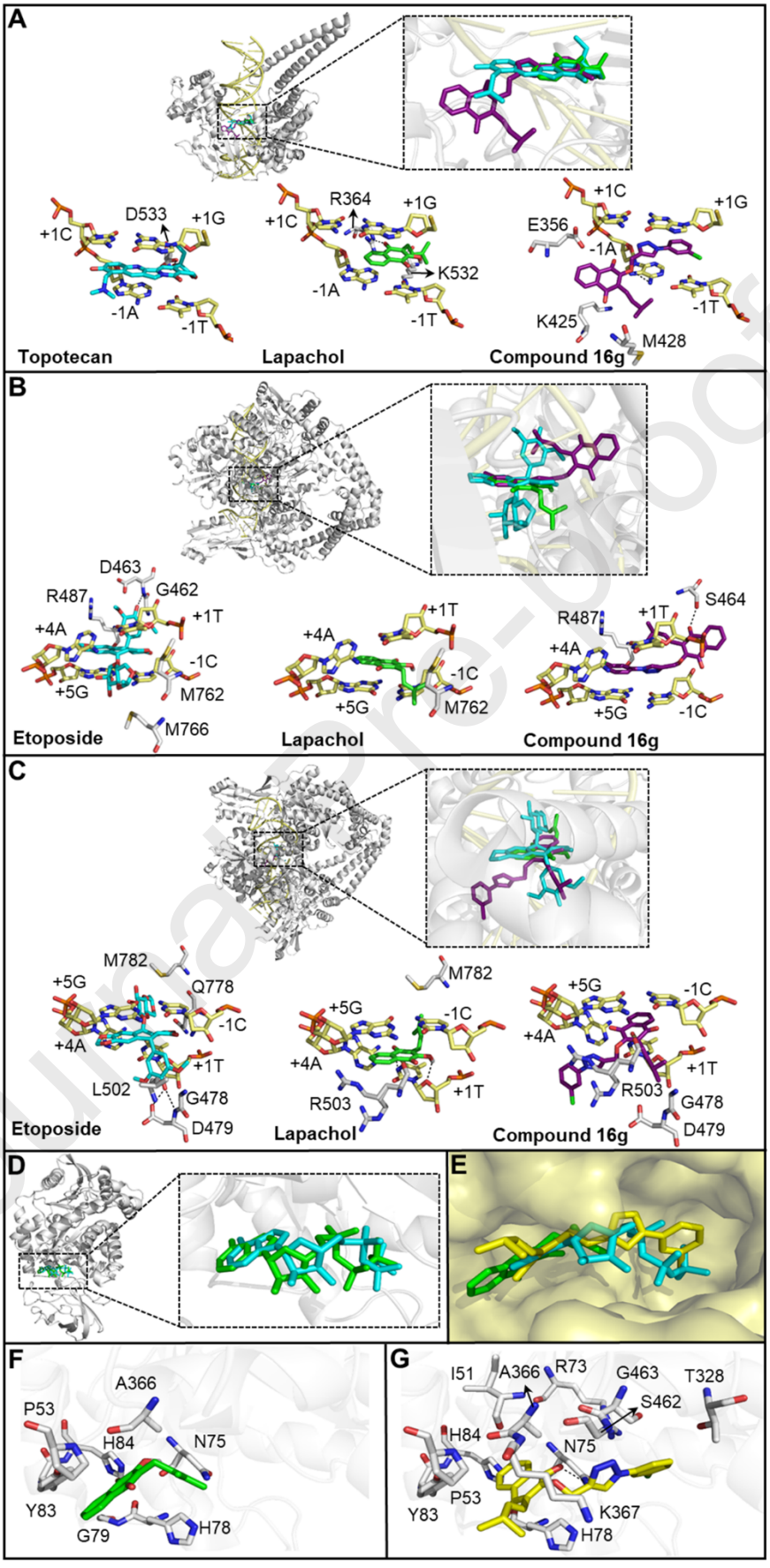
A
D533
+1G
+1C
-1A
-1T
Topotecan
R364
+1G
+1C
K532
-1A
-1T
Lapachol
+1C
+1G
E356
-1A
-1T
K425
M428
Compound 16g
B
D463
R487
G462
+1T
+4A
-1C
+5G
M762
M766
Etoposide
+1T
+4A
-1C
+5G
M762
Lapachol
R487
+1T
S464
+4A
+5G
-1C
Compound 16g
C
M782
+5G
Q778
-1C
+4A
+1T
L502
G478
D479
Etoposide
M782
+5G
-1C
+4A
+1T
R503
Lapachol
+5G
-1C
+4A
+1T
R503
G478
D479
Compound 16g
D
E
F
A366
P53
H84
N75
Y83
G79
H78
G
I51
A366
R73
G463
T328
S462
H84
N75
P53
Y83
K367
H78

Fig. 4. Compound 16g binds to topoisomerases and hPKM2 with high affinity. Binding mode of lapachol (green) and its derivative **16g** (purple) with DNA-binding domain of (A) topoisomerase I, (B) topoisomerase IIα, and (C) topoisomerase IIβ and comparison with the known inhibitors (cyan; topotecan for topoisomerase I and etoposide for topoisomerases IIα and IIβ). Carbon atoms of amino acid residues are shown in white while the C-atoms of nucleotides are shown in light yellow. (D) Redocking of ATP with rabbit muscle pyruvate kinase (PDB code 1A49), where experimental and docked poses are represented as green and cyan sticks, respectively. (E) Superposition of ATP conformation bound to rabbit muscle pyruvate kinase (cyan) and the docked poses of lapachol (green) and **16g** (yellow) bound within the active site of hPKM2. Binding mode and interactions of (F) lapachol (**3**), and (G) **16g** with hPKM2 obtained by molecular docking. Hydrogen bond interactions are shown as dashed lines. For more information and results see Supplementary Data.

PKM2 is an enzyme involved in the production of pyruvate and ATP at the last step of glycolysis. Pyruvate is then oxidized to produce ATPs in the presence of oxygen or converted to lactate when oxygen level is low. In cancer, cells increase their uptake of glucose and produce large amounts of pyruvate, which produce lactate independently of oxygen concentration. This occurs to attend their high energetic and biosynthetic needs. PKM2 is one of the proteins overexpressed in this situation [44]. PKM2 has already been linked to enhancing metastatic potential [45, 46], cancer invasion [47] and cancer progression [48] in OSCC. Indeed, PKM2 is overexpressed in OSCC tissue [47, 49, 50], being related to a poor survival of patients [47, 49]. Lapachol is a compound that target PKM2 and, as shown suggested in by the molecular docking results, compound **16g** may also theoretically bind had lower binding free energy (higher affinity) to PKM2 than Lapachol. Besides, lapachol (**3**) may present dose limiting toxicity [51]. Therefore, new drugs that can inhibit PKM2 activity are needed for both clinic and research, and compound **16g** may prove useful in this context.

Cell death pathway determination

Microtubule disorganization and inhibition of topoisomerases and PKM2 activities can induce different types of cell death, such as autophagy and apoptosis [52-55]. Thus, we investigated these two processes in our experimental context.

First of all, there was no relevant difference in LC3 stanning, an autophagy marker, between treatment and control (Supplementary **Fig. S4**). However, through time-lapse videomicroscopy images, it was observed that compound **16g** greatly increased the rate of detachment of SCC-9 cells when compared with control (**Fig. 5A**; Supplementary **Video S5**) and induced an increase in cellular blebs after 30 min. of treatment (**Fig. 5B**; Supplementary **Video S6**). It is worth to note that this phenotype occurs prior to cytoskeletal microtubule alteration observed before (**Fig. 3**). After 8 hours of treatment, there was a drastic change in cell morphology, with the shrinkage of cells and the formation of large membrane blebs, indicators of apoptosis (**Fig. 5B**). Besides, we tested for the presence of pyknotic nuclei and cleaved caspase-3 involvement, well-known apoptosis hallmarks. **Fig. 5C-D** shows a significant increase in the number of pyknotic nuclei on SCC-9 cells treated with compound **16g**, compared to control. The change in cell morphology under this treatment was also notable (**Fig. 5C**). The expression of cleaved caspase-3 in cells treated with compound **16g** was remarkable, in contrast to control (**Fig. 5E**). In more detail, these treated cells presented characteristic morphology of apoptosis, with cellular blebs and cell shrinkage (**Fig. 5F**). MTT assays using caspase inhibitors, ZVAD (pan-caspases) and ZDEVD (caspase-3), before incubation with compound **16g** showed an increase in cell viability compared to **16g** alone, specially ZVAD (**Fig. 5G**). In these assays, the total time of incubation with drugs was 24 hours, in contrast to the 30 minutes of incubation in the immunocytochemistry for cleaved caspase-3. The difference between results of ZVAD and ZDEVD might be explained because there is more than just one effector caspase (e.g. caspases 6) that have different substrate preference than DEVD (VEID) and thus are less sensitive to this inhibitor. Altogether, our results demonstrate that compound **16g** induces cell death through apoptosis.

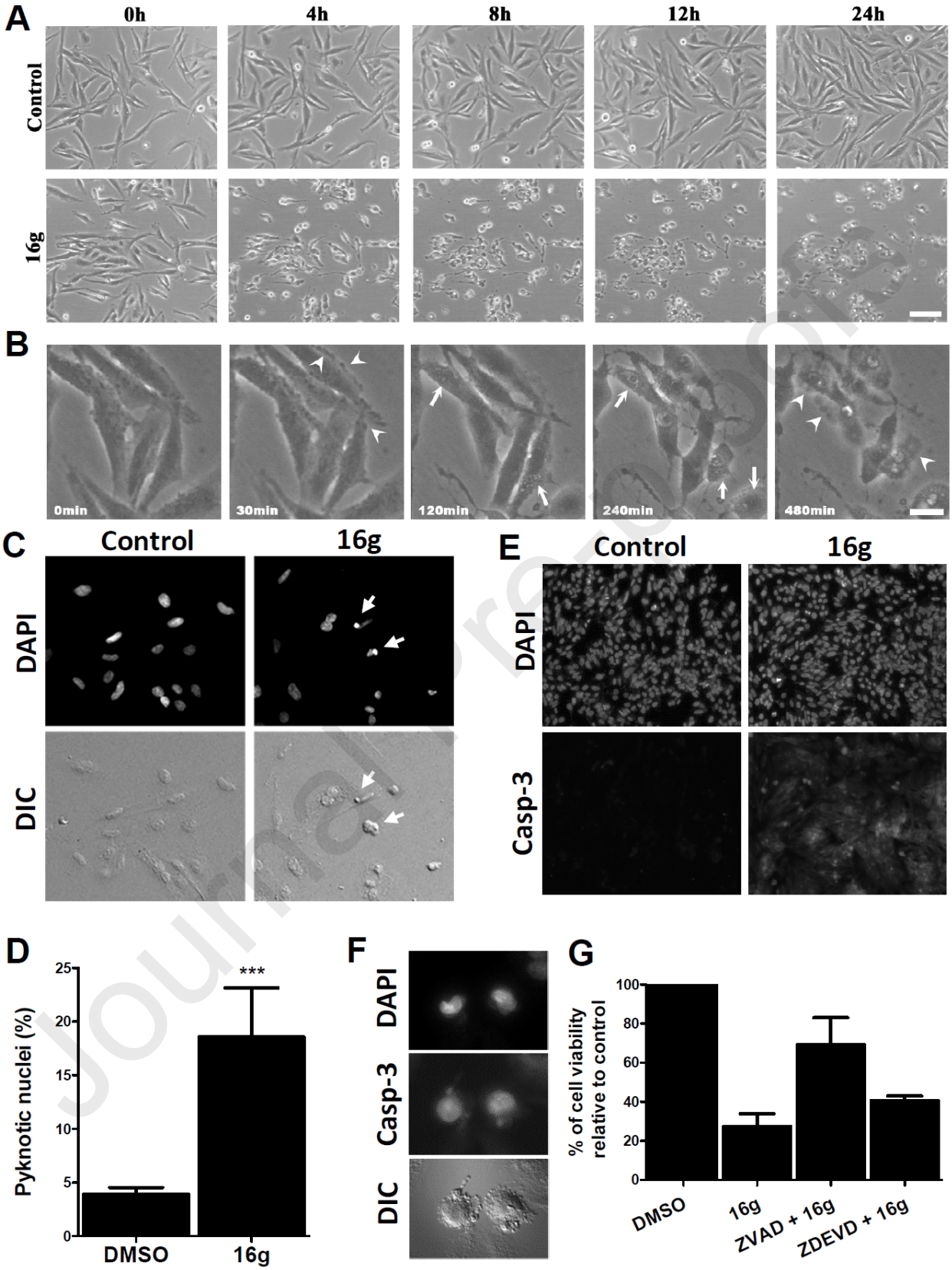

Fig. 5. Compound 16g induces cell death through apoptosis. All experiments were made using SCC9 cells. (A) Time-lapse videomicroscopy images obtained from Supplementary **Video S5** reveal that **16g** (2 x IC_{50}) increases the rate of detachment of SCC-9 cells when compared with control. Scale Bar is 100 μm. (B) Time-lapse videomicroscopy zoom obtained from Supplementary **Video S6** reveals that **16g** induced an increase in cellular blebs after 30min of treatment (indicated as white arrowheads). Between 120 and 240 min. after treatment, cells showed an increase in number and size of vacuoles (indicated as white arrows) together with a change in cell morphology, that drastically increased at 480 min. after treatment, with cell shrinkage and the formation of large membrane blebs (indicated as white arrowheads). Scale Bar is 20 μm. (C and D) Cells treated with 2 x IC_{50} of compound **16g** were stained with DAPI and had their pyknotic nuclei counted (representatives indicated with white arrows). (E and F) Immunocytochemistry of cleaved caspase-3 and detailed morphology of SCC-9 cells treated with 2 x IC_{50} for 30 minutes. DIC stands for Differential interference contrast microscopy. (G) MTT assay on SCC-9 cells using caspase inhibitors (pan-caspase – ZVAD; caspase 3 – ZDEVD) with 1 x IC_{50} of compound **16g** for 24 h. Results of at least 3 independent experiments.

4. Conclusions

In summary, thirty-five compounds of triazole naphthoquinones were synthesized and evaluated for their antitumor activity against OSCC. Classical chemotherapy pathways of action were tested, such as cytoskeletal dynamic alteration, DNA interaction, ROS production and topoisomerases inhibition. We found one of these compounds, **16g**, as highly effective, presenting high cytotoxicity (~ 35μM), selectivity (SI ~ 6) and low acute toxicity on animals. Mechanistically, compound **16g** induced apoptosis in OSCC cells, and disrupted the microtubule organization possibly by inhibition of activities of topoisomerases and hPKM2.

Acknowledgments

The authors would like to acknowledge the agencies that fund our research: CNPq (National Council of Research of Brazil), CAPES, FAPERJ. Fellowships granted by CNPq (305454/2017-0) and FAPERJ (E-26/203.191/2017, E-26/010.101106/2018) are gratefully

acknowledged. This study was financed in part by the Coordenação de Aperfeiçoamento de Pessoal de Nível Superior - Brasil (CAPES) - Finance Code 001.

Legal aspects

Animal use was authorized by *Comissão de Ética no Uso de Animal* from Universidade Federal Fluminense with registry number 982.

Conflict of interest

The authors declare no conflict of interest.

References

Declaration of interests

☒ The authors declare that they have no known competing financial interests or personal relationships that could have appeared to influence the work reported in this paper.

☐The authors declare the following financial interests/personal relationships which may be considered as potential competing interests:

Highlights

- Thirty-five new compounds of triazole naphthoquinones were synthesized.
- Compounds **16a**, **16b** and **16g** were able to induce cytotoxicity in human OSCC cell lines.
- Compound **16g** showed the higher SI value on cells and low toxic effects on mice.
- Compound **16g** induces apoptosis and acts on the microtubule, topoisomerases and hPKM2.
- **16g** might be considered as a lead compound for future cancer therapy.

In vitro

Compound	Oral tumor cells							Primary Gingival Fibroblast		Average S.I.
	SCC4		SCC9		SCC25		Average IC_{50}			
	IC_{50}	S.D.	IC_{50}	S.D.	IC_{50}	S.D.		IC_{50}	S.D.	
Carboplatin	316.70	0.52	268.3	0.03	270.80	0.46	266.90	394.10	0.04	1.37
Lapachol	158.10	0.01	77.27	0.11	171.00	0.07	135.46	211.90	0.02	1.56
16g	28.84	0.25	66.06	0.34	9.81	0.18	34.90	209.90	0.16	6.01

In vivo

Treatment	Dose mg/kg	Change in Body weight	Change in Food Consumption	Morbidity	Mortality	Gross Necropsy	Histology
Control	0	Absent	Absent	Absent	Absent	No alteration	Normal
16g	50	Absent	Absent	Absent	Absent	No alteration	Normal
	150	Absent	Absent	Absent	Absent	No alteration	Normal
	450	Absent	Absent	Absent	Absent	No alteration	Moderate megalocytosis; Moderate hepatocyte Binucleation

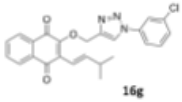

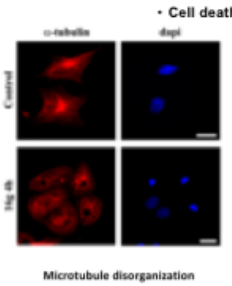

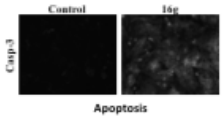

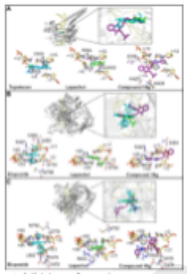

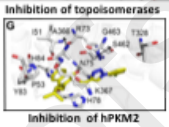

[1] R.L. Siegel, K.D. Miller, A. Jemal, Cancer statistics, 2019. CA Cancer J. Clin. 69 (2019) 7-34.

[2] F. Bray, J. Ferlay, I. Soerjomataram, R.L. Siegel, L.A. Torre, A. Jemal, Global cancer statistics 2018: GLOBOCAN estimates of incidence and mortality worldwide for 36 cancers in 185 countries. CA Cancer J. Clin. 68 (2018) 394-424.

[3] H. Yang, X. Jin, H. Dan, Q. Chen, Histone modifications in oral squamous cell carcinoma and oral potentially malignant disorders. Oral Dis. (2019). In Press. https://doi.org/10.1111/odi.13115

[4] J.D. McDermott, D.W. Bowles, Epidemiology of Head and Neck Squamous Cell Carcinomas: Impact on Staging and Prevention Strategies. Curr. Treat Options Oncol. 20 (2019) 43.

[5] C.M. Lewis, G.S. Ajmani, A. Kyrillos, P. Chamberlain, C.H. Wang, C.C. Nocon, M. Peek, M.K. Bhayani, Racial disparities in the choice of definitive treatment for squamous cell carcinoma of the oral cavity. Head Neck 40 (2018) 2372-2382.

[6] B.C. Zorzanelli, L.N. de Queiroz, R.M. Santos, L.M. Menezes, F.C. Gomes, V.F. Ferreira, F.C. da Silva, B.K. Robbs, Potential cytotoxic and selective effect of new benzo[*b*]xanthenes against oral squamous cell carcinoma. Future Med. Chem. 10 (2018) 1141-1157.

[7] F.C. da Silva, V.F. Ferreira, Natural Naphthoquinones with Great Importance in Medicinal Chemistry. Curr. Org. Synth. 13 (2016) 334-371.

[8] P.F. Carneiro, M.C.R.F. Pinto, R.K.F. Marra, F.C. da Silva, J.A.L.C. Resende, L.F.R. e Silva, H.G. Alves, G.S. Barbosa, M.C. de Vasconcellos, E.S. Lima, A.M. Pohlit, V.F. Ferreira. Synthesis and antimalarial activity of quinones and structurally-related oxirane derivatives. Eur. J. Med. Chem. 108 (2016) 134-140.

[9] A. Baramee, A. Coppin, M. Mortuaire, L. Pelinski, S. Tomavo, J. Brocard, Synthesis and in vitro activities of ferrocenic aminohydroxynaphthoquinones against *Toxoplasma gondii* and *Plasmodium falciparum*. Bioorg. Med. Chem. 14 (2006) 1294-302.

[10] S.C. Bourguignon, H.C. Castro, D.O. Santos, C.R. Alves, V.F.Ferreira, I.L. Gama, F.C. Silva, W.S. Seguins, R.T. Pinho, *Trypanosoma cruzi*: in vitro activity of Epoxy-α-Lap, a derivative of α-lapachone, on trypomastigote and amastigote forms. Exp. Parasitol. 122 (2009) 91-96.

[11] A.I. Francisco, M.D. Vargas, T.P. Fragoso, J.W.M. Carneiro, A. Casellato, F.C. da Silva, V.F. Ferreira, J.P. Barbosa, C. Pessoa, L.V. Costa-Lotufo, J.D.B. Marinho Filho, M.O. de Moraes, A.S. Mangrich, Theoretical studies of the tautomerism in 3-(2-R-Phenylhydrazono)-naphthalene- 1,2,4-triones: synthesis of copper(II) complexes and studies of antibacterial and antitumor activities.

Braz. Chem. Soc. 21 (2010) 1293-1302.

[12] N.M. Rahmoun, Z. Boucherit-Otmani, K. Boucherit, M. Benabdallah, D. Villemin, N. Choukchou-Braham, Antibacterial and antifungal activity of lawsone and novel naphthoquinone derivatives. Med. Mal. Infect. 42 (2012) 270-275.

[13] W. Li, X. Li, M. Liu, Q. Wang, Synthesis and Antiproliferative Activity of Thioxoflavones Mannich Base Derivatives. Arch. Pharm. 350 (2017) e1700044.

[14] V.P. Glazunov, D.V. Berdyshev, A. Yakubovskaya, N.D. Pokhilo, Chemistry of naphthazarin derivatives 13. Conformational analysis of 3-(alk-1-enyl)-2-hydroxy-1,4-naphthoquinones by quantum chemistry methods. Russ. Chem. Bull. 55 (2006) 1729-1736.

[15] L.F. Fieser, M. Fieser, Naphthoquinone Antimalarials. XII. The Hooker Oxidation Reaction. J. Am. Chem. Soc. 70 (1948) 3215-3222.

[16] S.B. Ferreira, D.R. da Rocha, J.W.M. Carneiro, W.C. Santos, V.F. Ferreira, A New Method to Prepare 3-Alkyl-2-hydroxy-1,4-naphthoquinones. Synthesis of Lapachol and Phthiocol. Synlett 11 (2011) 1551-1554.

[17] T.F. Borgati, J.D. de Souza Filho, A.B. de Oliveira. A complete and unambiguous 1H and 13C NMR signals assignment of para-naphthoquinones, ortho- and para-furanonaphthoquinones. J. Braz. Chem. Soc. 30 (2019) 1138-1149.

[18] N. Kongkathip, B. Kongkathip, P. Siripong, C. Sangma, S. Luangkamin, M. Niyomdecha, S. Pattanapa, S. Piyaviriyagul, P. Kongsaeree, Potent antitumor activity of synthetic 1,2-Naphthoquinones and 1,4-Naphthoquinones. Bioorg. Med. Chem. 11 (2003) 3179-3191.

[19] D.R. da Rocha, K. Mota, I.M.C.B. da Silva, V.F. Ferreira, S.B. Ferreira, F.C. da Silva., Synthesis of fused chromene-1,4-naphthoquinones via ring-closing metathesis and Knoevenagel-electrocyclization under acid catalysis and microwave irradiation. Tetrahedron 70 (2014) 3266-3270.

[20] W.O. Valença, T.V. Baiju, F.G. Brito, M.H. Araujo, C. Pessoa, B.C. Cavalcanti, C.A. de Simone, C. Jacob, I.N.N. Namboothiri, E.N. da Silva Júnior. Synthesis of Quinone-Based N-Sulfonyl-1,2,3-triazoles: Chemical Reactivity of Rh(II) Azavinyl Carbenes and Antitumor Activity. Chemistry Select 2 (2017) 4301-4308.

[21] N. Boechat, V.F. Ferreira, S.B. Ferreira, M.L.G. Ferreira, F.C. da Silva, M.M. Bastos, M.S. Costa, M.C.S. Lourenço, A.C. Pinto, A.U. Krettli, A.C. Aguiar, B.M. Teixeira, N.V. da Silva, P.R.C. Martins, F.A.F.M. Bezerra, A.L.S. Camilo, G.P. da Silva, C.C.P. Costa, Novel 1,2,3-Triazole Derivatives for Use against *Mycobacterium tuberculosis* H37Rv (ATCC 27294) Strain, J. Med. Chem. 54 (2011) 5988-5999.

[22] D.T.G. Gonzaga, L.B.G. Ferreira, T.E.M.M. Costa, N.L. von Ranke, P.A.F. Pacheco, A.P.S. Simões, J.C. Arruda, L.P. Dantas, H.R. de Freitas, R.A.M. Reis, C. Penido, M.L. Bello, H.C. Castro, C.R. Rodrigues, V.F. Ferreira, R.X. Faria, F.C. da Silva, 1-Aryl-1H- and 2-aryl-2H-1,2,3-triazole derivatives blockade P2X7 receptor *in vitro* and inflammatory response *in vivo*. Eur J Med Chem. 139 (2017) 698-717.

[23] B.L. Staker, K. Hjerrild, M.D. Feese, C.A. Behnke, A.B. Burgin Jr, L. Stewart, The mechanism of topoisomerase I poisoning by a camptothecin analog. Proc. Natl. Acad. Sci. USA. 99 (2002) 15387-15292.

[24] Y.R. Wang, S.F. Chen, C.C. Wu, Y.W. Liao, T.S. Lin, K.T. Liu, Y.S. Chen, T.K. Li, T.C. Chien, N.L. Chan, Producing irreversible topoisomerase II-mediated DNA breaks by site-specific Pt(II)-methionine coordination chemistry. Nucleic Acids Res. 45 (2017) 10861-1087.

[25] C.C. Wu, T.K. Li, L. Farh, L.Y. Lin, T.S. Lin, Y.J. Yu, T.J. Yen, C.W. Chiang, N.L. Chan, Structural basis of type II topoisomerase inhibition by the anticancer drug etoposide. Science. 333 (2011) 459-462.

[26] O. Trott, A.J. Olson, AutoDock Vina: improving the speed and accuracy of docking with a new scoring function, efficient optimization and multithreading, J. Comput. Chem. 31 (2010) 455-461.

[27] D.C.S. Costa, G.S. de Almeida, V.W. Rabelo, L.M. Cabral, P.C. Sathler, P.A. Abreu, V.F. Ferreira, L.C.R.P. da Silva, F.C. da Silva, Synthesis and evaluation of the cytotoxic activity of Furanaphthoquinones tethered to 1H-1,2,3-triazoles in Caco-2, Calu-3, MDA-MB231 cells. Eur. J. Med. Chem. 156 (2018) 524-533.

[28] T.M. Larsen, M.M. Benning, I. Rayment, G.H. Reed, Structure of the bis(Mg2+)-ATP-oxalate complex of the rabbit muscle pyruvate kinase at 2.1 A resolution: ATP binding over a barrel. Biochemistry 37 (1998) 6247-6255.

[29] A.L. Macedo, D.P.D. da Silva, D.L. Moreira, L.N. de Queiroz, T.R.A. Vasconcelos, G.F. Araujo, M.A.C. Kaplan, S.S.C. Pereira, E.C.P. de Almeida, A.L. Valverde, B.K. Robbs, Cytotoxicity and selectiveness of Brazilian Piper species towards oral carcinoma cells. Biomed Pharmacother. 110 (2019) 342-352.

[30] R.B. Badisa, S.F. Darling-Reed, P. Joseph, J.S. Cooperwood, L.M. Latinwo, C.B. Goodman, Selective cytotoxic activities of two novel synthetic drugs on human breast carcinoma MCF-7 cells. Anticancer Res. 29 (2009) 2993-2996.

[31] D.F. Basri, Z.A. Alamin, K.M. Chan, Assessment of cytotoxicity and genotoxicity of stem bark extracts from Canarium odontophyllum Miq. (dabai) against HCT 116 human colorectal cancer cell line. BMC Complement Altern. Med. 16 (2016) 36.

[32] S.C. Stone, F.A. Vasconcellos, E.J. Lenardão, R.C. do Amaral, R.G. Jacob, F.P. Leivas Leite, Evaluation of potential use of Cymbopogon sp. essential oils, (R)-citronellal and N-citronellylamine in cancer chemotherapy. Int. J. Appl. Res. Nat. Prod. 6 (2013) 11-15.

[33] N.A. Franken, H.M. Rodermond, J. Stap, J. Haveman, C. van Bree, Clonogenic assay of cells in vitro. Nat. Protoc. 1 (2006) 2315-9.

[34] S. Parasuraman, Toxicological screening. J. Pharmacol. Pharmacother. 2 (2011) 74-79.

[35] Y.J. Schneider, R. Baurain, A. Zenebergh, A. Trouet, DNA-binding parameters of daunorubicin and doxorubicin in the conditions used for studying the interaction of anthracycline-DNA complexes with cells in vitro. Cancer Chemother. Pharmacol. 2 (1979) 7-10.

[36] J.J. Vicente, L. Wordeman, The quantification and regulation of microtubule dynamics in the mitotic spindle. Curr. Opin. Cell Biol. 60 (2019) 36-43.

[37] K.E. Arnst, S. Banerjee, H. Chen, S. Deng, D.J. Hwang, W. Li, D.D. Miller, Current advances of tubulin inhibitors as dual acting small molecules for cancer therapy. Med. Res. Rev. 39 (2019) 1398-1426.

[38] B.S. Kumar, K. Ravi, A.K. Verma, K. Fatima, M. Hasanain, A. Singh, J. Sarkar, S. Luqman, D. Chanda, A.S. Negi, Synthesis of pharmacologically important naphthoquinones and anticancer activity of 2-benzyllawsone through DNA topoisomerase-II inhibition. Bioorg. Med. Chem. 25 (2017) 1364-1373.

[39] A. Esteves-Souza, D.V. Figueiredo, A. Esteves, C.A. Câmara, M.D. Vargas, A.C. Pinto, A. Echevarria, Cytotoxic and DNA-topoisomerase effects of lapachol amine derivatives and interactions with DNA. Braz. J. Med. Biol. Res. 40 (2007) 1399-402.

[40] H. Xu, Q. Chen, H. Wang, P. Xu, R. Yuan, X. Li, L. Bai, M. Xue, Inhibitory effects of lapachol on rat C6 glioma in vitro and in vivo by targeting DNA topoisomerase I and topoisomerase II. J. Exp. Clin. Cancer Res. 35 (2016) 178.

[41] C. Zhang, Y. Qu, B. Niu, Design, synthesis and biological evaluation of lapachol derivatives possessing indole scaffolds as topoisomerase I inhibitors. Bioorg. Med. Chem. 24 (2016) 5781-5786.

[42] K. Hevener, T.A. Verstak, K.E. Lutat, D.L. Riggsbee, J.W. Mooney, Recent developments in topoisomerase-targeted cancer chemotherapy. Acta Pharm. Sin. B. 8 (2018) 844-861.

[43] M.S. Babu, S. Mahanta, A.J. Lakhter, T. Hato, S. Paul, S.R. Naidu, Lapachol inhibits glycolysis in cancer cells by targeting pyruvate kinase M2. PLoS One. 13 (2018) e0191419.

[44] S. Amin, P. Yang, Z. Li, Pyruvate kinase M2: A multifarious enzyme in non-canonical localization to promote cancer progression. Biochim. Biophys. Acta Rev. Cancer. 1871 (2019) 331-341.

[45] W. Wang, Q. He, J. Sun, Z. Liu, L. Zhao, Z. Lu, X. Zhou, A. Wang, Pyruvate kinase M2 deregulation enhances the metastatic potential of tongue squamous cell carcinoma. Oncotarget 8 (2017) 68252-68262.

[46] W. Wang, Q. He, W. Yan, J. Sun, Z. Chen, Z. Liu, Z. Lu, J. Hou, Y. Shao, X. Zhou, A. Wang, High glucose enhances the metastatic potential of tongue squamous cell carcinoma via the PKM2 pathway. Oncotarget 8 (2017) 111770-111779.

[47] Y.J. Park, J.Y. Kim, D.Y. Lee, X. Zhang, S. Bazarsad, W.Y. Chung, J. Kim, PKM2 enhances cancer invasion via ETS-1-dependent induction of matrix metalloproteinase in oral squamous cell carcinoma cells. PLoS One. 14 (2019) e0216661.

[48] F. Tanaka, S. Yoshimoto, K. Okamura, T. Ikebe, S. Hashimoto, Nuclear PKM2 promotes the progression of oral squamous cell carcinoma by inducing EMT and post-translationally repressing TGIF2. Oncotarget 9 (2018) 33745-33761.

[49] Y. Wang, X. Zhang, Y. Zhang, Y. Zhu, C. Yuan, B. Qi, W. Zhang, D. Wang, X. Ding, H. Wu, J. Cheng, Overexpression of pyruvate kinase M2 associates with aggressive clinicopathological features and unfavorable prognosis in oral squamous cell carcinoma. Cancer Biol. Ther. 16 (2015) 839-845.

[50] T.S. Wong, X.B. Liu, H.A. Chung-Wai, Y.A. Po-Wing, Ng Wai-Man, W.W. Ignace, Identification of pyruvate kinase type M2 as potential oncoprotein in squamous cell carcinoma of tongue through microRNA profiling. Int. J. Cancer. 123 (2008) 251-257.

[51] H. Hussain, I.R. Green, Lapachol and lapachone analogs: a journey of two decades of patent research (1997-2016). Expert Opin. Ther. Pat. 27 (2017) 1111-1121.

[52] B. Chu, J. Wang, Y. Wang, G. Yang, Knockdown of PKM2 induces apoptosis and autophagy in human A549 alveolar adenocarcinoma cells. Mol. Med. Rep. 12 (2015) 4358-4363.

[53] F. Mollinedo, C. Gajate, Microtubules, microtubule-interfering agents and apoptosis. Apoptosis. 8 (2003) 413-450.

[54] S. Olivier, Q.A. Khan, K.W. Kohn, Y. Pommier, Apoptosis Induced by Topoisomerase Inhibitors. Curr. Med. Chem. - Anti-Cancer Agents. 3 (2003) 271-290.

[55] R.J. Wei, S.S. Lin, W.R. Wu, L.R. Chen, C.F. Li, H.D. Chen, C.T. Chou, Y.C. Chen, S.S. Liang, S.T. Chien, Y.L. Shiue, A microtubule inhibitor, ABT-751, induces autophagy and delays apoptosis in Huh-7 cells. Toxicol. Appl. Pharmacol. 311 (2016) 88-98.